Redox Biology 14 (2018) 100–115

Contents lists available at ScienceDirect

Redox Biology

journal homepage: www.elsevier.com/locate/redox

Research Paper

# Iron accumulation in senescent cells is coupled with impaired ferritinophagy and inhibition of ferroptosis

Shashank Masaldan[a], Sharnel A.S. Clatworthy[a], Cristina Gamell[b], Peter M. Meggyesy[a], Antonia-Tonia Rigopoulos[a], Sue Haupt[b,c], Ygal Haupt[b,c,d], Delphine Denoyer[a], Paul A. Adlard[e], Ashley I. Bush[e], Michael A. Cater[a,d,*]

[a] Centre for Cellular and Molecular Biology, School of Life and Environmental Sciences, Deakin University, Burwood, Victoria 3125, Australia
[b] Research Division, Peter MacCallum Cancer Centre, East Melbourne, Victoria 3002, Australia
[c] The Sir Peter MacCallum Department of Oncology, The University of Melbourne, Parkville, Victoria 3010, Australia
[d] Department of Pathology, The University of Melbourne, Parkville, Victoria 3010, Australia
[e] The Florey Institute of Neuroscience and Mental Health, The University of Melbourne, Parkville, Victoria 3052, Australia

ARTICLE INFO

*Keywords:*
Senescence
Iron
Ferritinophagy
Ferroptosis
Ferritin
Autophagy
Ageing

ABSTRACT

Cellular senescence is characterised by the irreversible arrest of proliferation, a pro-inflammatory secretory phenotype and evasion of programmed cell death mechanisms. We report that senescence alters cellular iron acquisition and storage and also impedes iron-mediated cell death pathways. Senescent cells, regardless of stimuli (irradiation, replicative or oncogenic), accumulate vast amounts of intracellular iron (up to 30-fold) with concomitant changes in the levels of iron homeostasis proteins. For instance, ferritin (iron storage) levels provided a robust biomarker of cellular senescence, for associated iron accumulation and for resistance to iron-induced toxicity. Cellular senescence preceded iron accumulation and was not perturbed by sustained iron chelation (deferiprone). Iron accumulation in senescent cells was driven by impaired ferritinophagy, a lysosomal process that promotes ferritin degradation and ferroptosis. Lysosomal dysfunction in senescent cells was confirmed through several markers, including the build-up of microtubule-associated protein light chain 3 (LC3-II) in autophagosomes. Impaired ferritin degradation explains the iron accumulation phenotype of senescent cells, whereby iron is effectively trapped in ferritin creating a perceived cellular deficiency. Accordingly, senescent cells were highly resistant to ferroptosis. Promoting ferritin degradation by using the autophagy activator rapamycin averted the iron accumulation phenotype of senescent cells, preventing the increase of TfR1, ferritin and intracellular iron, but failed to re-sensitize these cells to ferroptosis. Finally, the enrichment of senescent cells in mouse ageing hepatic tissue was found to accompany iron accumulation, an elevation in ferritin and mirrored our observations using cultured senescent cells.

## 1. Introduction

Cellular senescence refers to cells that have undergone irreversible growth arrest through replicative exhaustion, or in response to a variety of pro-oncogenic cellular stresses (e.g. oncogenes, oxidants, and radiation) [1,2]. Irrespective of the stimulus, senescence safeguards against the unrestricted growth of damaged cells and promotes cellular clearance through eliciting the immune system. However, senescent cells accumulate with age and contribute to chronic diseases and age-related dysfunctions, in part, through the pro-inflammatory factors (e.g. cytokines & chemokines) they secrete (senescence-associated secretory phenotype; SASP) [1,2]. Senescent cells and SASP have been linked with chronic inflammation that is often observed during ageing in tissues in the absence of obvious infection [2]. The clearance of senescent cells in mice, using a novel transgene (*INK-ATTAC*) that allows for selective apoptosis of p16-positive senescent cells in vivo, improved healthspan by attenuating age-related pathologies both prophylactically and as treatment [3,4]. Removal of p16-positive senescent cells in ageing mice delayed tumourigenesis and attenuated age-related deterioration of several organs, including kidney, heart and adipose tissue, without adverse side effects [3]. Furthermore, a median lifespan extension was observed, indicating that p16-positive senescent cells negatively impact longevity [3].

Senolytic (anti-senescence) treatment is also sought-after for cancer therapy, as current chemotherapeutics (e.g. DNA damaging agents) can cause cancer cells to become senescent [5–8]. Senescent cells are linked

* Corresponding author at: Centre for Cellular and Molecular Biology, School of Life and Environmental Sciences, 221 Burwood Highway, Burwood, VIC 3125, Australia.
*E-mail addresses:* mcater@deakin.edu.au, mcater@unimelb.edu.au (M.A. Cater).

http://dx.doi.org/10.1016/j.redox.2017.08.015
Received 10 August 2017; Received in revised form 21 August 2017; Accepted 22 August 2017
Available online 01 September 2017

with cancer drug resistance and recurrence [9,10]. A novel senolytic agent (FOXO4-p53 interfering peptide) has shown promise in mice, promoting apoptosis of doxorubicin-induced senescent cells, neutralizing doxorubicin-induced toxicity and improving overall healthspan [6]. Together, these studies demonstrate tangible health benefits for targeting senescent cells and thereby identify senescent cells as being integral to many age-related pathologies and dysfunctions.

Several reports have described dysfunctional iron homeostasis with ageing, either systemically [11,12], or in specific organ systems affected by age-related pathologies [13–15]. Age-dependent accumulation of iron in various tissues has been reported to occur separately to the enrichment of senescent cells [11,12,16–19]. Diseases associated with the accumulation of senescent cells, such as neurodegenerative disorders (e.g. Alzheimer's and Parkinson's) [20–22], osteoarthritis [23,24] and idiopathic pulmonary fibrosis [25], also exhibit iron dyshomeostasis where often iron burden correlates with disease severity [14,15,26–34]. Iron accumulation occurs in replicative senescent fibroblasts in vitro [35] and the iron storage protein ferritin is enriched in ageing tissues [36,37]. Since excess iron can be toxic through redox activity, iron burden has been hypothesized to cause cellular damage or to promote ferroptosis. However, the relationship between senescent cells and iron dyshomeostasis in ageing, or in age-related pathologies, is unclear. We therefore investigated whether altered iron homeostasis is a characteristic of senescent cells using mammalian cell culture models and aged wild-type (wt) C57BL/6 mice. The aim was to determine if the senescence phenotype is intrinsically linked with changes to cellular iron homeostasis and related cell death pathways.

## 2. Results

### 2.1. Senescent cells accumulate large amounts of intracellular iron

We initially studied a well-established model of cellular senescence in mouse embryonic fibroblasts (MEFs) induced by sublethal gamma irradiation [38,39]. The DNA damage incurred sequentially activates the p53-p21 and p16-RB effector pathways, representing distinct phases from early to full senescence [2,40]. When cultured for ≥ 10 days, more than 80% of irradiated MEFs (MEF IR) stained positive for senescence associated beta-galactosidase (SA-βgal) activity (Fig. 1**A(i),**Fig. S1A). Senescent MEFs remain viable (Fig. S1B) and can be metabolically active in culture for many months [2]. To permit sufficient time for a net change in intracellular iron to occur, we cultured irradiated MEFs (MEF IR) for 21 days, by which time they expressed increased p53 and p16 protein expression consistent with senescence incurred through DNA damage (Fig. 1**A(ii)**). Transcripts for senescent markers, p16, p21 and IL-6 were also increased (Fig. S1C). Intracellular iron was measured by inductively-coupled plasma mass spectrometry (ICP-MS) and at 21 days post-irradiation senescent MEFs (MEF IR) accumulated a large amount of iron (~ 20-fold) when compared to primary non-irradiated MEFs (MEF PRI) (Fig. 1**A(iii)**). The iron accumulation was reliant on p53-mediated senescence induction and was not indirectly caused by irradiation (Fig. S1E). One consequence of cellular senescence is the reported morphological change in cell size (flat-cell phenotype) [41], which is an important factor to consider when quantifying intracellular metals. Consistent with previous reports [41], the diameter of adhered senescent MEFs (at 21 days post-irradiation) was approximately twice that of primary non-irradiated MEFs (MEF PRI) (Fig. S1F). However, diameters of suspended cells measured following dissociation of adherent cells were closely aligned (Fig. S1G). Cellular protein content is considered a surrogate marker for overall cell size, increasing roughly linearly with cell mass and volume [42]. Total cellular protein was slightly elevated (~ 1.3-fold) in senescent MEFs (MEF IR) (Fig. S1G), but could not account for the magnitude of increased intracellular iron (~ 20-fold) (Fig. 1**A(iii)**).

To ascertain whether intracellular iron accumulation occurs when senescence is induced through other stimuli, not just through irradiation, we measured iron in MEFs that underwent replicative senescence (REP), or oncogene ($HRas^{V12}$) induced senescence (OIS). In our hands, replicative senescence in primary MEFs occurred at passage 7 (P7), as established through staining for SA-βgal activity (10 days post-seeding) (Fig. 1**B(i)**) and was accompanied with termination of their replicative potential [population doubling limit (PDL) < 0.2] (Fig. S1H). When MEFs at passage 7 were sustained in culture for 21 days they had increased p53 and p16 expression (Fig. 1**B(ii)**). Concurrently, these replicative senescent MEFs (MEF REP), analogous to irradiation-induced senescent MEFs (MEF IR) (Fig. 1**A),** accumulated a vast amount of intracellular iron (~ 20-fold) (Fig. 1**B(iii)**). Variation in cell diameter or total cellular protein content between primary (MEF PRI) and replicative senescent MEFs (MEF REP) did not account for the degree of increased intracellular iron (Fig. S1F, G). In contrast, the well-characterised NIH(3T3) MEF line, that spontaneously bypassed senescence (43), had intracellular iron levels more comparable to that of primary MEFs (MEF PRI) despite multiple passages (Fig. 1**B(iii)**). We aided isogenic MEFs (our embryo lineage) to spontaneously bypass senescence by using the 3T3 culturing method [ISO(3T3)] [43] and these cells also had minimal change in their cellular iron content (Fig. 1**B(iv)**). Furthermore, primary MEFs immortalised with retrovirus containing SV40 large T antigen (MEF-LT) (at passage 5) (Fig. 1**B(v)**), evaded replicative senescence and continually proliferated, but maintained intracellular iron levels comparable to those of primary MEFs (MEF PRI) (Fig. 1**B(vi)**). Therefore, iron accumulation is associated with replicative senescence in MEFs and is not a feature of MEFs that have either spontaneously bypassed senescence or were immortalised.

Oncogene-induced senescence (OIS) was produced in MEFs by using retroviruses containing $HRas^{V12}$ (Fig. 1**C**). $HRas^{V12}$ directly causes senescence by activating the MAPK pathway in murine fibroblasts, arresting cells at the G1 cell cycle stage and is accompanied by an accumulation of p53 and p16 [44]. Oncogene-induced senescence has also been linked to the reactivation of programmed developmental senescence involving p21 and p15 and thus has molecular distinctions from replicative and irradiation-induced senescence that emanate from DNA damage response (DDR) mechanisms [45]. Senescent MEFs (MEF OIS) were determined by SA-βgal activity 8 days after retroviral transduction with $HRas^{V12}$ and represented approximately 50% of the cell population (Fig. 1**C(i)**). Despite the limited percentage of senescent cells the accumulation of intracellular iron (~ 4.5-fold) was still evident when compared to MEFs transduced with control retroviruses (Fig. 1**C(ii)**). Immortalised primary MEFs (MEF-LT) transduced with retroviruses containing $HRas^{V12}$ showed no signs of cellular senescence and accordingly no iron accumulation (Fig. 1**C(ii)**).

Cellular senescence can be induced by different molecular mechanisms depending upon the cell type and species of origin [2]. We therefore further demonstrated that human primary diploid fibroblast (HDFs) and prostate epithelial cells (PrECs), analogous to MEFs, also accumulated intracellular iron following senescence induction through either irradiation (IR) (Fig. 2**A**) or replicative exhaustion (REP) (Fig. 2**B**). Taken together, these results demonstrate that intracellular iron accumulates in senescent cells irrespective of stimuli, or cell origin (mouse vs. human; fibroblast vs. epithelial) and is therefore possibly a universal feature.

### 2.2. Altered iron homeostatic mechanisms drive senescent cells to acquire profound levels of intracellular iron

The remarkable increase in intracellular iron in senescent cells would conceivably necessitate numerous adaptive changes by the cell. Iron represents a double-edged sword, as its redox property that is utilised by many biochemical reactions also renders it potentially toxic. Iron can catalyse the production of reactive oxygen species (ROS) and free radicals, including the highly reactive hydroxyl radical [46]. We therefore investigated the levels of key cellular iron homeostasis proteins in senescent MEFs (21 days post-irradiation) (Fig. 3). Western blot

analyses revealed that senescent MEFs (MEF IR) had significantly elevated levels of transferrin receptor 1 (TfR1), the principle protein responsible for the cellular uptake of iron via transferrin ($Fe^{3+}$-transferrin) (Fig. 3**A**). The divalent metal transporter 1 (DMT1) protein, which is involved in transport of iron ($Fe^{2+}$) from endosomes to cytoplasm, did not significantly change (Fig. 3**A**). Ferroportin was also increased in senescent cells (Fig. 3**A**) and can function to efflux iron from the cell under certain conditions. However, in senescent cells ferroportin predominantly localized to an intracellular compartment and not at the plasma membrane (Fig. S2A–C) and therefore is unlikely to partake in effective iron efflux. Strikingly, the cellular iron storage protein, ferritin, was elevated more than 10-fold in senescent cells (Fig. 3**A**). Considering that each ferritin complex is capable of coordinating up to 4500 atoms of iron [47,48], a 10-fold increase in protein levels could easily account for the iron accumulation in senescent cells and for its detoxification. To ascertain whether ferritin also increased markedly in senescent cells of other origins, we utilised both human primary diploid fibroblast (HDFs) and prostate epithelial cells (PrECs). When senescent (21 days post-irradiation), these human cell lines both displayed a substantial increase in intracellular ferritin (Fig. 3**B(i),(ii)**), consistent with concurrent iron accumulation (Fig. 2). Additionally, when senescence in MEFs was induced through continual passaging (REP), there was likewise a marked elevation in ferritin (Fig. 3**B(iii)**) corresponding to the iron accumulation (Fig. 1**B**).

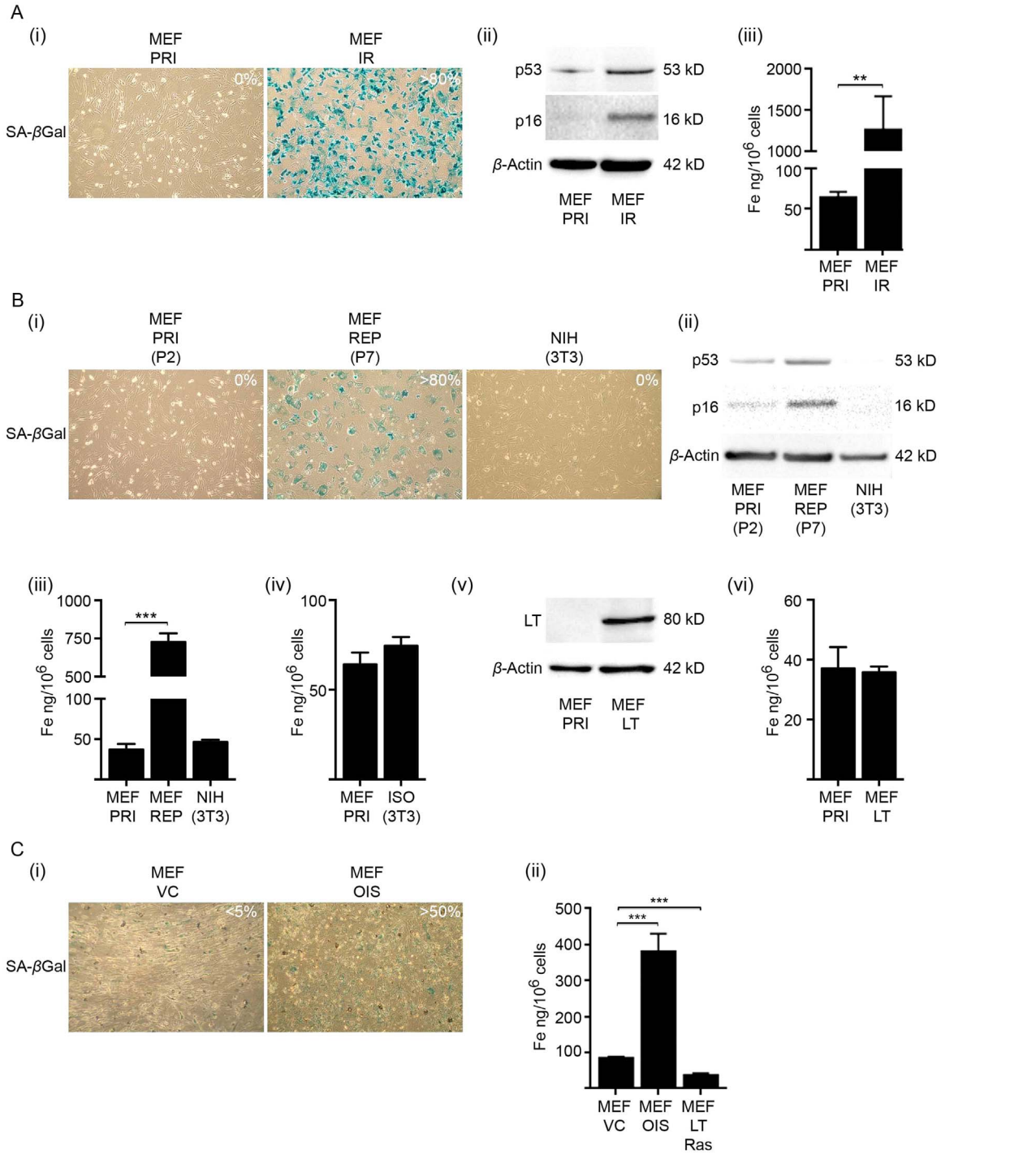


*(caption on next page)*

**Fig. 1.** Senescent MEFs accumulate vast amounts of intracellular iron. **(A)** Induction of senescence in MEFs by sublethal gamma irradiation (10 Gy) caused intracellular iron accumulation. **(i)** Percentage of senescent MEFs in primary (MEF PRI) and irradiated (MEF IR) cultures as determined by SA-βgal activity. The majority (> 80%) of MEFs displayed positive SA-βgal activity 10 days post-irradiation (IR) (blue staining). Images were taken at 100× magnification. **(ii)** Western blot analyses of molecular markers of senescence, p53 and p16, in primary (PRI) and irradiated (IR) MEFs. Senescent MEFs (MEF IR) had elevated levels of both p53 and p16 at 21 days post-irradiation (10 Gy). β-actin was detected as a loading control. **(iii)** ICP-MS analyses demonstrated that senescent MEFs (MEF IR) accumulated intracellular iron (~ 20-fold) at 21 days post-irradiation (10 Gy). Note that media were replenished weekly. **(B)** Induction of senescence in MEFs by replicative exhaustion caused intracellular iron accumulation. **(i)** Percentage of senescent MEFs in primary (MEF PRI), replicative senescent (MEF REP) and senescence-bypassed NIH(3T3) cultures. The majority (> 80%) of MEFs became replicative senescent (REP) at passage 7 (10-days post seeding), being positive for SA-βgal activity (blue staining). Senescence-bypassed NIH(3T3) cells had no detectable SA-βgal activity. Images were taken at 100× magnification. **(ii)** Western blot analyses of molecular markers of senescence, p53 and p16, in primary (MEF PRI), replicative senescent (MEF REP) and senescence-bypassed [NIH(3T3)] MEFs. Replicative senescent MEFs (MEF REP) when cultured for 21 days at passage 7 had elevated levels of both p53 and p16. β-actin was detected as a loading control. **(iii)** ICP-MS analyses demonstrated that replicative senescent MEFs (REP) when cultured for 21 days at passage 7 accumulated intracellular iron (~ 20-fold). MEFs that underwent senescence-bypass [NIH(3T3)] had intracellular iron levels comparable to that of primary MEFs (MEF PRI). **(iv)** ICP-MS analyses demonstrated that isogenic MEFs that we aided to spontaneously bypass senescent [ISO(3T3)] also had intracellular iron level comparable to that of primary MEFs (MEF PRI). **(v)** Primary MEFs were immortalised with virus containing the SV40 large T antigen (LT). Western blot analyses confirmed LT expression at passage 7 post-immortalisation. β-actin was detected as a loading control. **(vi)** ICP-MS analyses demonstrated that immortalised MEFs (MEF LT) at passage 7 had intracellular iron levels comparable to that of primary MEFs (MEF PRI). **(C)** Induction of senescence in MEFs with virus containing the oncogene *H-Ras$^{V12}$* caused intracellular iron accumulation. **(i)** Percentage of senescent MEFs in primary (PRI) and oncogenic-induced senescent MEFs (OIS) as determined by SA-βgal activity. MEFs transduced with virus containing *H-Ras$^{V12}$* (OIS) were enriched for SA-βgal positive cells (> 50%) at 8 days post-transduction in comparison to MEFs transduced with control virus (VC) (< 5%). Images were taken at 100× magnification. **(ii)** ICP-MS analyses demonstrated that oncogenic-induced senescent MEFs (OIS) accumulated intracellular iron (~ 4.5-fold) at 8 days post-transduction with virus containing *H-Ras$^{V12}$*. Immortalised MEFs [LT(SV40)] transduced with virus containing *H-Ras$^{V12}$* (MEF LT Ras) had intracellular iron levels comparable to that of primary MEFs (PRI). Statistical analysis was performed by student-*t*-test: significant (*$p < 0.05$, **$p < 0.01$, ***$p < 0.001$). Data represented as mean ± SD ($n = 3$).

Therefore, ferritin may be a marker of cellular senescence and associated iron accumulation.

The principal regulators of cellular iron homeostasis are the iron regulatory proteins (IRPs), IRP1 and IRP2. These proteins bind to iron-responsive elements (IRE) situated in mRNAs of key iron homeostasis proteins. During iron deficiency, IRPs bind to ferritin and ferroportin mRNAs to repress translation and to TfR1 mRNAs to block its degradation. In excess iron, IRPs do not bind, increasing the expression of ferritin and ferroportin while promoting TfR1 mRNA degradation [48]. Senescent MEFs (MEFs IR) had significantly lower levels of both IRP1 and its regulator the iron-sulfur cluster assembly enzyme (ISCU) (Fig. 3**C**), which is required for iron-sulfur cluster biogenesis [48–50]. IRP1 when bound with an iron-sulfur (4Fe-4S) cluster functions as a cytosolic aconitase instead of a translational regulator [48,49]. However, senescent MEFs (MEF IR) had markedly elevated IRP2 expression, consistent with having elevated TfR1 but not with elevated ferritin and ferroportin (Fig. 3**A**). Unlike IRP1, IRP2 is regulated via iron-dependent degradation and acts as a sensor for cellular iron bioavailability [48]. Furthermore, the IRE-binding activity of IRP2 correlates with its protein level [48,51,52]. Therefore, high levels of IRP2 are usually indicative of decreased cellular iron bioavailability. Taken together, these results demonstrate that iron accumulation in senescent cells is associated with dramatic changes in the levels of relevant homeostatic proteins; with a paradoxical increase in both TfR1 and ferritin coupled with internalized ferroportin.

### *2.3. Cellular senescence precedes iron accumulation and provides resistance to iron induced toxicity*

We next sought to determine the timeframe between cellular senescence development and iron accumulation and whether augmented iron levels are maintained in metabolically active senescent cells. Occurrence of the senescence phenotype (SA-βgal activity) and iron accumulation was surveyed in MEFs at time intervals following irradiation (1, 7, 14 and 21 days) (Fig. 4**A, B**). Media were replenished weekly for each time point. The accumulation of intracellular iron (Fig. 4**B**) occurred in parallel with the formation of senescent cells and reflected the percentage of senescent cells at days 7 (> 50%) and 14 (> 80%) post-irradiation (Fig. 4**A**). However, the amount of accumulated iron between days 14 and 21 plateaued. A similar limit for iron accumulation was demonstrated in replicative senescent MEFs (Fig. S3). This upper threshold was reflected by the protein levels of both TfR1 and ferritin, which increased until, and peaked at, 14 days post-irradiation (Fig. 4**C**). To establish whether the level of iron accumulation at 14 days post-irradiation represented sequestration capacity, we treated senescent MEFs (MEF IR) at this time point with either basal medium or media supplemented with 5 μM or 40 μM iron [as ferric ammonium citrate (FAC)] for 24 h (Fig. 4**D**). Primary non-irradiated MEFs (MEF PRI) were treated equivalently as a control (Fig. 4**D**). Remarkably, there was a further dose-dependent increase in the capacity of senescent MEFs to accumulate iron, with cells accumulating up to ~ 3-fold more (with 40 μM FAC) when compared with senescent cells cultured in basal medium and ~ 30-fold more when compared with primary MEFs cultured in basal medium (Fig. 4**D**).

Analogous to the response documented in most cell types, primary MEFs with augmented intracellular iron (following 24 h FAC treatments) (Fig. 4**D**) had reduced TfR1 and upregulated ferritin in order to counteract toxicity (Fig. 4**E(i)**). However under the same treatment conditions, senescent MEFs (14 days post-irradiation) further increased TfR1 (5 μM FAC) and likewise ferritin (Fig. 4**E(ii)**). Ferritin continued to increased even when senescent MEFs, already laden with intracellular iron, were exposed to media containing pathological levels of iron (40 μM FAC). These ferritin dynamics seen in senescent MEFs would conceivably enhance resistance to iron. Consistent with this idea, senescent MEFs (14 days post-irradiation) were substantially less vulnerable to iron induced toxicity than primary non-irradiated MEFs (MEF PRI) (Fig. 4**F**). Therefore, homeostatic mechanisms in senescent MEFs are geared for continual uptake and sequestration of milieu iron and afford cells resistance to toxicity from excess iron.

We wondered whether iron accumulation mediates cellular senescence (Fig. 4**G–H**). Primary MEFs were treated with the cell-permeable iron chelator deferiprone (Dfp) (50 μM) while irradiated (10 Gy) to become senescent and then subsequently for 10 days in culture. Note that 10 days in culture is required for > 80% of irradiated MEFs (MEF IR) to stain positive for SA-βgal activity (Figs. 1**A(i),**4**A**). Sustained Dfp treatment inhibited both intracellular iron accumulation and ferritin upregulation in the irradiated MEFs (MEF IR) (Fig. 4**G(i),(ii)**), but did not inhibit senescence development (Fig. 4**H**). Once senescence was fully established (21 days post-irradiation) Dfp treatment (50 μM for 24 h) could only marginally decrease intracellular iron and consequently had a negligible effect on ferritin level (Fig. 4**I(i), (ii)**). Stored iron in senescent cells once accumulated is therefore highly resistant to removal. Taken together, these results demonstrate that iron accumulation occurs post-senescence development and is associated with remarkable ferritin dynamics that confer resistance to iron-induced toxicity.

### *2.4. Iron accumulation in senescent MEFs is associated with impaired ferritinophagy and inhibition of ferroptosis*

Ferritinophagy, the process of ferritin being sequestered into autophagosomes and delivered to lysosomes for degradation, is important for liberating iron from ferritin and thus for maintaining cellular iron homeostasis [51,53–55]. We hypothesized that impaired ferritin

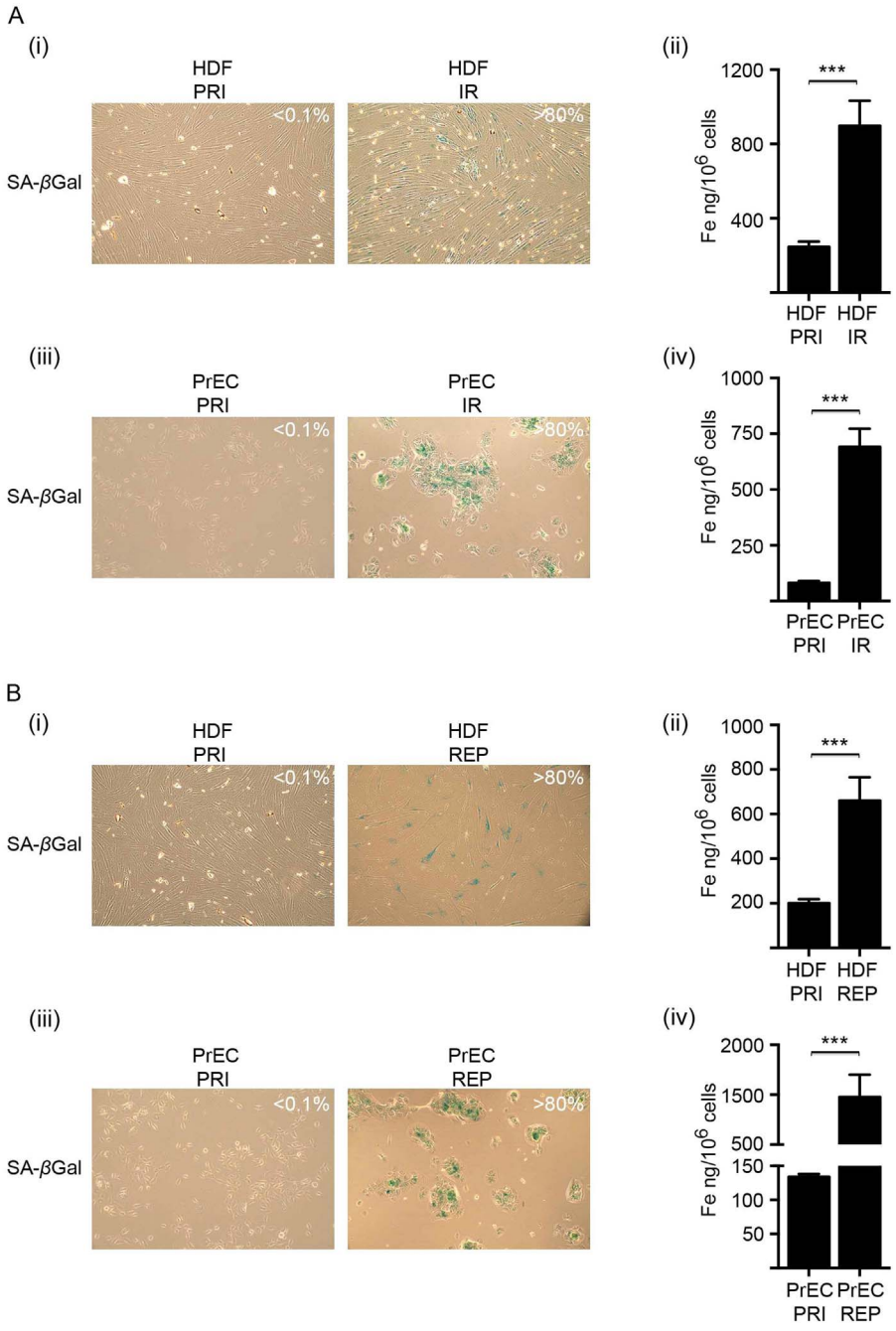


**Fig. 2.** Human senescent cells from different linages (fibroblast or epithelial) accumulate vast amounts of intracellular iron. **(A)** Induction of senescence in human diploid fibroblasts and human prostate epithelial cells by irradiation (IR, 10 Gy) caused intracellular iron accumulation. **(i)** Percentage of senescent diploid fibroblasts in primary (HDF PRI) and irradiated (HDF IR) cultures as determined by SA-βgal activity. The majority (> 80%) of diploid fibroblasts displayed positive SA-βgal activity 10 days post-irradiation (blue staining). Images were taken at 100× magnification. **(ii)** ICP-MS analyses demonstrated that senescent diploid fibroblasts (HDF IR) accumulated intracellular iron (~ 3.6-fold) at 21 days post-irradiation. **(iii)** Percentage of senescent human prostate epithelial cells in primary (PrEC PRI) and irradiated (PrEC IR) cultures as determined by SA-βgal activity. The majority (> 80%) of prostate epithelial cells displayed positive SA-βgal activity 10 days post-irradiation (blue staining). Images were taken at 100× magnification. **(iv)** ICP-MS analyses demonstrated that senescent prostate epithelial cells (PrEC IR) accumulated intracellular iron (~ 8.4-fold) at 21 days post-irradiation. **(B)** Induction of senescence in human diploid fibroblasts and human prostate epithelial cells by replicative exhaustion caused intracellular iron accumulation. **(i)** Percentage of senescent diploid fibroblasts in primary (HDF PRI) and replicatively exhausted (HDF REP) cultures as determined by SA-βgal activity. The majority (> 80%) of diploid fibroblasts became replicative senescent (HDF REP) at passage 29, being positive for SA-βgal activity (blue staining). Images were taken at 100× magnification. **(ii)** ICP-MS analyses demonstrated that senescent diploid fibroblasts (HDF REP) when cultured for 21 days at passage 29 accumulated intracellular iron (~ 3.3-fold). **(iii)** Percentage of senescent prostate epithelial cells in primary (PrEC PRI) and replicatively exhausted (PrEC REP) cultures as determined by SA-βgal activity. The majority (> 80%) of prostate epithelial cells became replicative senescent (PrEC REP) at passage 6, being positive for SA-βgal activity (blue staining). Images were taken at 100× magnification. **(ii)** ICP-MS analyses demonstrated that senescent prostate epithelial cells (PrEC REP) when cultured for 21 days at passage 6 accumulated intracellular iron (~7.3-fold). Statistical analysis was performed by student-*t*-test: significant ($*p < 0.05$, $**p < 0.01$, $***p < 0.001$). Data represented as mean ± SD ($n = 3$).

degradation might explain the iron accumulation phenotype of senescent cells; by effectively trapping iron in ferritin and thereby creating a perceived cellular deficiency. To investigate this, we compared the lysosome-mediated ferritin degradation pathway of primary (MEF PRI) to senescent MEFs (MEF IR) (Fig. 5). Primary MEFs (MEF PRI) were treated with 40 μM iron (FAC) for 24 h to increase ferritin (Fig. 5**A(i)**), raising the intracellular iron concentrations to similar levels for senescent MEFs (MEF IR) (14 days post-irradiation) (Fig. 5**A(ii)**). Ferritin degradation was then stimulated with the iron chelator deferoxamine (Dfo) (50 μM) as previously described [51,53,56] and occurred substantially within 6 h of treatment (Fig. 5**A(i)**). The acidic environment of the lysosome is crucial for iron extraction from ferritin and for subsequent ferritin degradation [51]. Accordingly, we found that ferritin degradation was inhibited by alkalinisation of the lysosome with ammonium chloride ($NH_4Cl$) (Fig. 5**A(i)**). These results are consistent with lysosome-mediated ferritin degradation in MEFs as previously reported [51,54,55]. However, in senescent MEFs (14 days post-irradiation) the equivalent treatment with Dfo was insufficient to induce ferritin degradation (Fig. 5**B**), suggesting impairment of this pathway.

Lysosomal dysfunction has recently emerged as an important feature of oxidative stress-induced senescence and is characterised by the build-up of autophagosomes [36,57]. To confirm that senescent MEFs have impaired lysosomal function, we assessed the level of the membrane-bound form of microtubule-associated protein light chain 3 (LC3-II). LC3-II localizes to autophagosomes that ultimately fuse with lysosomes (autolysosomes) and is consequently degraded by lysosomal hydrolases [58,59]. Lysosomal dysfunction causes cells to markedly accumulate LC3-II in autophagic structures [58]. In cells with normal lysosomal activity (turnover) a higher ratio of LC3-II to its cytosolic (soluble) precursor LC3-I can indicate enhanced autophagy, due to greater autophagosome formation [58,59]. We used rapamycin (100 nM), which selectively activates autophagy through inhibiting the

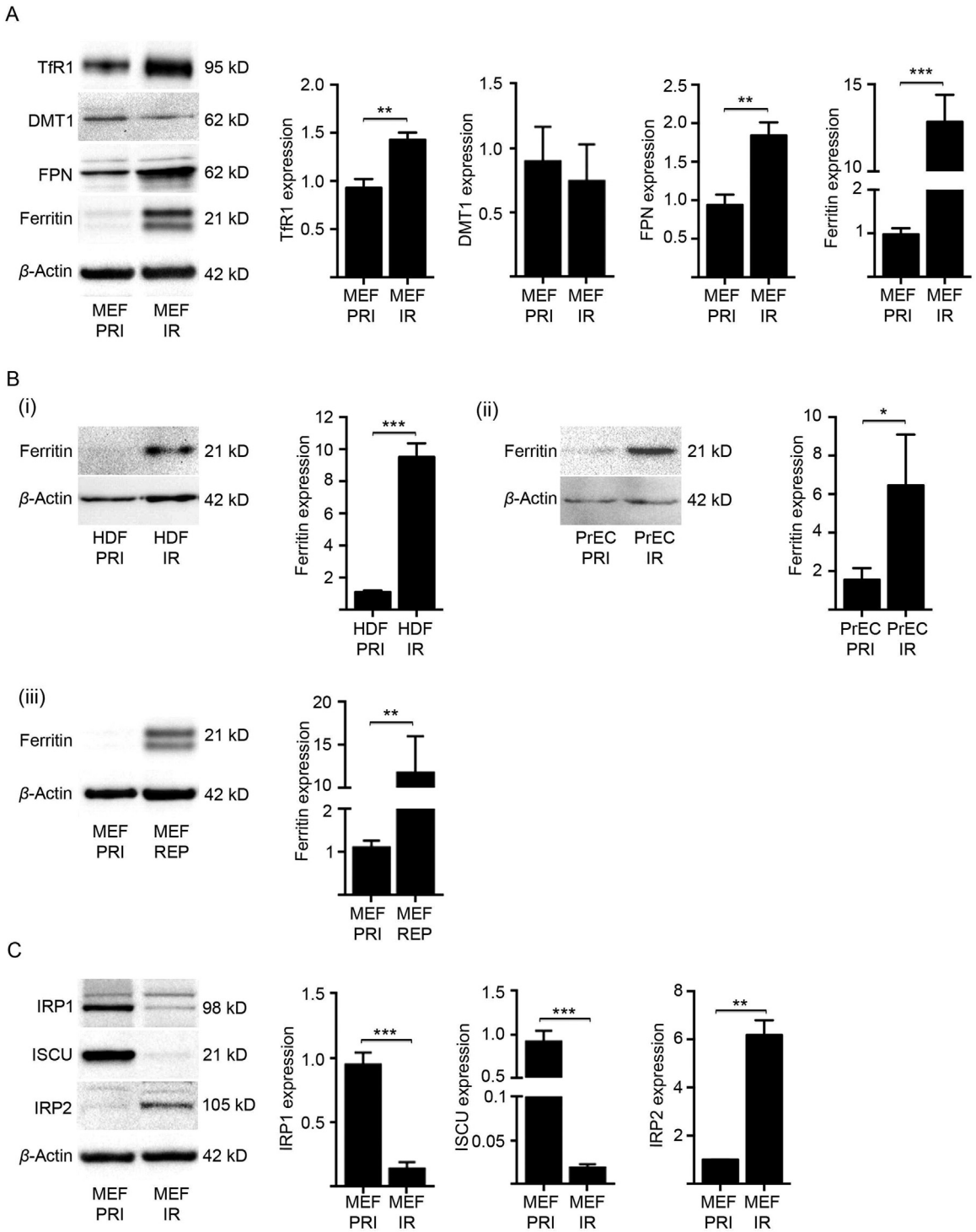


**Fig. 3.** Altered iron homeostatic mechanisms drive senescent cells to acquire intracellular iron. **(A)** Expression of key iron homeostasis proteins was analysed in senescent MEFs (IR) at 21 days post-irradiation (10 Gy) by western blot and densitometry. The levels of transferrin receptor 1 (TfR1) [main iron ($Fe^{3+}$) importer], divalent metal transporter 1 (DMT1) (cytosolic iron importer), ferroportin (iron exporter) and ferritin (intracellular iron storage) were measured in comparison to primary (PRI) MEFs. β-actin was detected as a loading control. **(B)** Western blot analyses and densitometry confirm elevated expression of ferritin in (**i**) senescent human diploid fibroblasts (HDF IR) and in **(ii)** senescent human prostate epithelial cells (PrEC IR), both at 21 days post-irradiation (10 Gy). Furthermore, elevated ferritin expression was confirmed in (**iii**) replicative senescent MEFs (P7) cultured for 21 days. β-actin was detected as loading controls. **(C)** Expression of key regulatory proteins of iron homeostasis was analysed in senescent MEFs (IR) at day 21 post-irradiation (10 Gy) by western blot and densitometry. The levels of iron regulatory protein 1 (IRP1) and iron-sulfur cluster assembly enzyme (ISCU) were found significantly lower than those in primary (PRI) MEFs, while IRP2 was significantly elevated. β-actin was detected as a loading control. Statistical analysis was performed by student-*t*-test: significant ($*p < 0.05$, $**p < 0.01$, $***p < 0.001$). Data represented as mean ± SD ($n = 3$).

mTOR pathway [60] to activate autophagy in primary MEFs (MEF PRI), significantly increasing the LC3-II: LC3-I ratio (Fig. 5**C**). In contrast, treatment with bafilomycin A1 (100 nM), an inhibitor of late-phase autophagy (prevents fusion of autophagosomes and lysosomes) [61], significantly reduced the LC3-II: LC3-I ratio (Fig. 5**C**). Note that level of LC3-II is enhanced in primary MEFs (MEF PRI) treated with bafilomycin A1, indicating that the concentration of bafilomycin A1 used was sufficient to diminish autophagic degradation of LC3-II. In senescent MEFs

(10 days post-irradiation) there was a large build-up of LC3-II, consistent with impaired lysosomal function (Fig. 5**D**). The fold-increase of LC3-II that accumulated in senescent MEFs (Fig. 5**D**) was much greater than that observed in primary MEFs treated with bafilomycin A1 (Fig. 5**C**). LC3-II also accumulated in replicative senescent MEFs (MEF REP), concomitant with elevated ferritin (Fig. S3C). LC3-II: LC3-I ratio is not a reliable indicator of autophagy in cells possessing dysfunctional lysosomes and so was not evaluated for the senescent cells [58]. To further confirm autophagic-lysosomal dysfunction in senescent MEFs, we measured endogenous levels of the p62 protein (Fig. 5**D**), which is normally turned over via this pathway. Elevated p62 levels were previously observed in oxidative stress-induced senescent cells [57], and consistent with this study, we demonstrated that our senescent MEFs (MEF IR) likewise had markedly elevated levels of p62 when compared

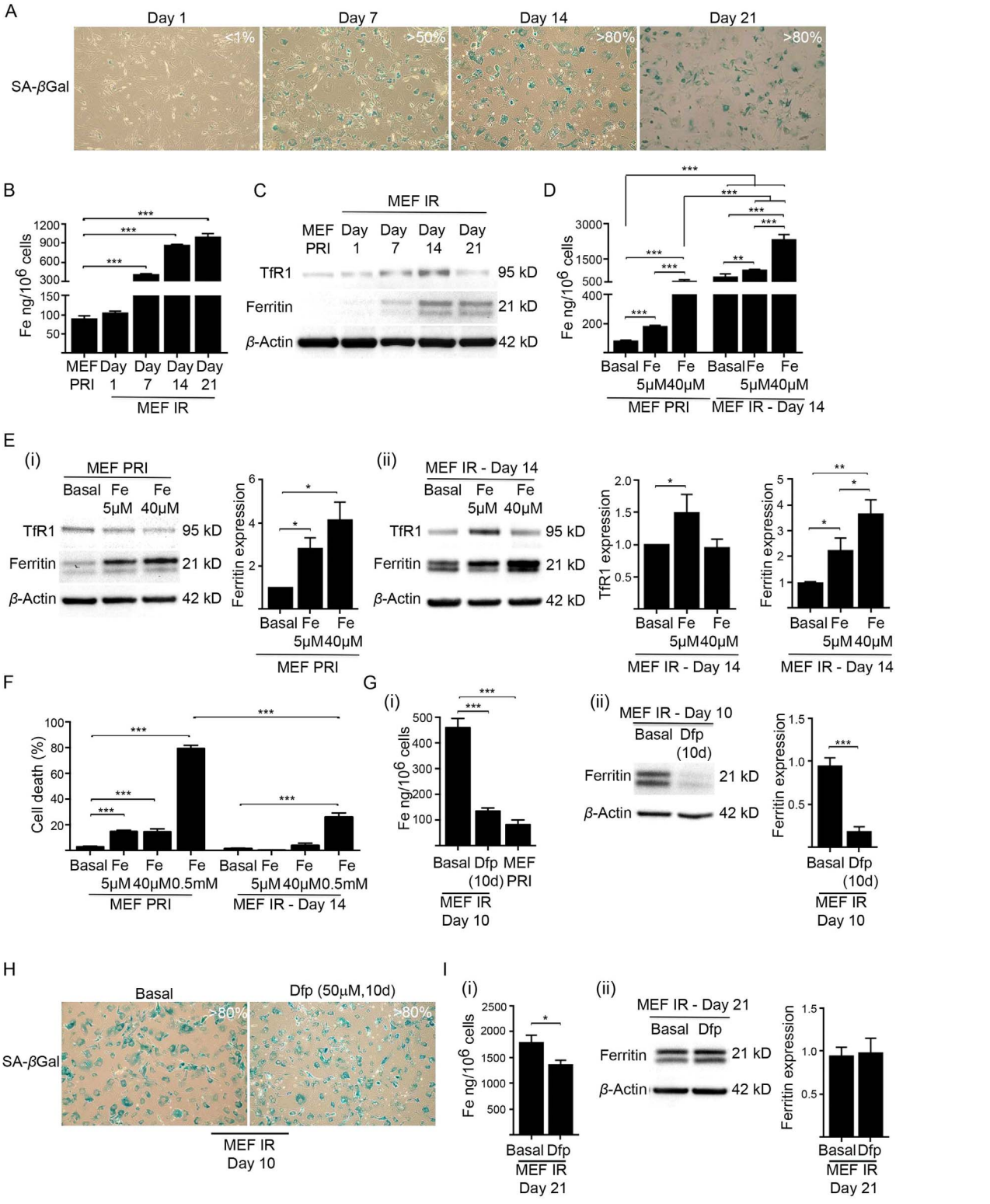


*(caption on next page)*

**Fig. 4.** Cellular senescence precedes iron accumulation and provides resistance to iron induced toxicity. **(A)** Percentage of senescent MEFs (MEF IR) post-irradiation (10 Gy) over the culturing time points indicated (day 1, 7, 14 and 21), as determined by SA-βgal activity (blue staining). Images were taken at 100× magnification. **(B)** ICP-MS analyses demonstrated cumulative intracellular iron accumulation in irradiated (10 Gy) senescent MEFs (MEF IR) over the culturing time points indicated (day 1, 7, 14 and 21). Note that iron accumulation somewhat plateaued after day 14, but was maintained. Baseline intracellular iron level in primary MEFs (MEF PRI) is also shown. **(C)** Expression of iron uptake and storage proteins was analysed in senescent MEFs (IR) post-irradiation (10 Gy) over the culturing time points indicated (day 1, 7, 14 and 21) by western blot. The levels of transferrin receptor 1 (TfR1) [main iron ($Fe^{3+}$) importer] and ferritin (intracellular iron storage) were determined in comparison to primary (PRI) MEFs. β-actin was detected as a loading control. **(D)** Capacity of senescent MEFs to accumulate iron is dependent on milieu iron concentration. Primary (PRI) MEFs or irradiated (10 Gy) senescent MEFs (IR) (cultured for 14 days) were cultured for 24 h in basal medium, or media supplemented with either 5 μM or 40 μM iron (FAC). ICP-MS analyses revealed a dose-dependent increase in accumulated iron in primary and senescent MEFs (IR) following iron treatment. **(E)** Senescent MEFs are geared to sequester milieu iron. **(i)** Western blot analyses demonstrated that TfR1 was downregulated and ferritin upregulated (fold change indicated by densitometry) when primary MEFs (MEF PRI) were cultured for 24 h in media supplemented with either 5 μM or 40 μM iron (FAC). **(ii)** Western blot analyses and densitometry demonstrated that TfR1 and ferritin are further upregulated when senescent cells (14 days post-irradiation) were cultured for 24 h in media supplemented with either 5 μM or 40 μM iron (FAC). β-actin was detected as loading controls. **(F)** Senescent MEFs possess enhanced resistance to elevated iron. The viability of iron treated primary and senescent MEFs was determined by propidium iodide and flow cytometry. Note that an extremely high concentration of iron (500 μM) was used as a positive control. **(G)** Chelation reduced intracellular iron and ferritin accumulation in irradiated MEFs. Primary MEFs were treated with the cell-permeable iron chelator deferiprone (Dfp) (50 μM) while irradiated (10 Gy) to become senescent and then subsequently for 10 days in culture. Primary MEFs irradiated and cultured in basal medium served as a control. **(i)** ICP-MS analyses demonstrated that sustained Dfp treatment prevented iron accumulation in irradiated MEFs. Baseline intracellular iron level in primary MEFs (MEF PRI) is also shown. **(ii)** Western blot analyses and densitometry demonstrated that sustained Dfp treatment prevented ferritin accumulation in irradiated MEFs. β-actin was detected as a loading control. **(H)** Percentage of senescent MEFs following sustained Dfp treatment. Primary MEFs were treated with Dfp (50 μM) while irradiated (10 Gy) to become senescent and then subsequently for 10 days in culture. Primary MEFs irradiated and cultured in basal medium served as a control. The majority (> 80%) of treated MEFs become senescent, staining positive for SA-βgal activity (blue staining).**(I)** Stored iron in senescent MEFs once accumulated is highly resistant to chelation. Senescent MEFs (21 days post-irradiation) treated with Dfp (50 μM) for 24 h showed **(i)** only a marginal decrease in intracellular iron as determined by ICP-MS. **(ii)** Western blot analyses and densitometry showed a negligible effect of Dfp treatment on ferritin level of senescent MEFs. β-actin was detected as a loading control. Statistical analysis was performed by student-*t*-test: significant ($*p < 0.05$, $**p < 0.01$, $***p < 0.001$). Data represented as mean ± SD ($n = 3$).

to primary MEFs (MEF PRI) (Fig. 5**D**). Together, these results confirmed autophagic-lysosomal dysfunction in senescent MEFs.

We examined senescent cells for their sensitivity to ferroptosis (Fig. 5**E**), an iron-dependent autophagic cell death program [62–64] that can be inhibited in MEFs by genetically inactivating autophagy or ferritinophagy [65]. We treated senescent MEFs (MEF IR and MEF REP) for 24 h with varying concentrations of erastin and RSL3 (0.1–5 μM), two structurally different inducers of ferroptosis that affect distinct pathways [66]. Senescent MEFs, both irradiated (MEF IR) and replicatively exhausted (MEF REP) were markedly resistant to ferroptosis in comparison to primary MEFs (MEF PRI) (Fig. 5**E(i)**). Taken together, these results demonstrate that lysosomal impairment is a feature of cellular senescence and is associated with ferritin accumulation (impaired ferritinophagy) and resistance to ferroptosis.

We next tested whether preserving lysosomal function in senescent cells would prevent the iron accumulation phenotype. The mTOR inhibitor rapamycin has been shown to restore lysosomal function in senescent cells [57]. The mTOR pathway is a negative regulator of autophagy and is implicated in cellular senescence [67], most notably through SA-βgal activity and the expression of p16 and p21 markers [67,68]. Primary MEFs were treated with rapamycin (100 nM) while irradiated (10 Gy) to induce senescence and also subsequently for 10 days in culture. Phosphorylated ribosomal protein S6 (pS6), a marker for mTOR activity, was significantly reduced in rapamycin treated cells (Fig. 5**F**). Loss of pS6 promotes autophagosome formation [69]. Sustained rapamycin treatment was associated with a reduction in LC3-II, indicating preservation of lysosomal function and permissible LC3-II degradation (Fig. 5**F**). Rapamycin also averted the iron accumulation phenotype of senescent MEFs, preventing the increase of TfR1, ferritin (Fig. 5**F**) and intracellular iron (Fig. 5**G**).

Rapamycin treatment suppressed SA-βgal activity (~ 50%) in irradiated cells (Fig. 5**H**), as expected [68], although the cells remained in a non-proliferative state (Fig. S4A). Additionally, once senescence was fully established (10 days post-irradiation) subsequent rapamycin treatment (100 nM for 4 days) significantly reduced the intracellular accumulation of iron (Fig. 5**I**) without affecting SA-βgal activity (Fig. S4B). Torin 1, another inhibitor of mTOR with a different mode of action to rapamycin [70], showed a similar capacity to reduce iron accumulation (Fig. S4C). Together these results demonstrate that cellular senescence is associated with impaired ferritinophagy, explaining the associated iron-accumulation phenotype.

We next tested whether averting the iron accumulation phenotype through rapamycin treatment (Fig. 5**F,G**) would restore the sensitivity of senescent MEFs (MEFs IR) to ferroptosis (Fig. 5**J**). Primary MEFs were again treated with rapamycin (100 nM) while irradiated (10 Gy) to induce senescence and then subsequently for 10 days in culture. Subsequently, these cells were treated ferroptosis-inducers erastin and RSL3 (0.1–5 μM) (Fig. 5**J**). Despite preserving ferritinophagy, rapamycin treatment was insufficient for sensitizing senescent cells to ferroptosis and therefore other overriding factors are likely involved in impeding ferroptosis in these cells.

### 2.5. Ageing mice accumulate senescent liver cells with iron and ferritin

Having established that senescent cells in vitro accumulate large amounts of iron, we next investigated whether similar changes occur in ageing mice, which have previously been reported to accumulate senescent cells in various organs/tissues [3]. We focused on the ageing mouse liver, as senescence within this organ has been well characterised and detection through SA-βgal activity was shown to have negligible background [38]. Consistent with previous reports, there was a significant increase (~ 10-fold) in the percentage of SA-βgal positive cells in histological liver sections of 30 month-old mice (Aged) (C57BL/6; $n = 4$), when compared to 3 month-old mice (Young) (C57BL/6; $n = 4$) (Fig. 6**A**). ICP-MS analyses demonstrated that aged mouse livers, in addition to accumulating senescent cells, also accumulated iron (~ 2.6-fold) (Fig. 6**B**). Western blot analyses revealed that in senescence-enriched aged livers, in accordance with there being elevated iron levels, there was also elevated levels of the iron-storage protein, ferritin (Fig. 6**C(i)**). The increase in ferritin in aged livers positively correlated with increased p16 protein and transcript levels (Fig. 6**C(i),(ii)**), which served as a further marker for cellular senescence in addition to SA-βgal activity staining (Fig. 6**A**). Serial histological liver sections from both young ($n = 3$) and aged mice ($n = 3$) were then stained for cellular senescence (SA-βgal activity) and ferritin (Fig. 6**D**). Consistent with the western blot analyses (Fig. 6**C**), there was augmented levels of ferritin in histological liver sections of aged mice when compared to young mice (Fig. 6**D**). Note that the ferritin antibody was diluted in these experiments to facilitate the exclusive detection of ferritin overexpressing cells. Additionally, the percentage of ferritin-enriched cells within aged livers (~ 10%) (Fig. 6**D**) corresponded well with the percentage of SA-βgal positive senescent cells (~ 11%) (Fig. 6**A**). Taken together, the enrichment of senescent cells in ageing hepatic tissue was found to accompany iron accumulation, an elevation in the iron-storage ferritin protein and mirrored our observations in vitro using cultured senescent cells.

## 3. Discussion

Senescent cells can impair tissue function in ageing despite their

relatively low abundance (< 15%) [3,4]. However, how senescent cells exert adverse effects is poorly understood. We have provided mechanistic insight into a novel activity of senescent cells, relating to altered iron acquisition and storage. Intracellular iron accumulation was identified as a hallmark of cellular senescence irrespective of the inducing stimuli (IR, REP or OIS) (Fig. 1) and occurred across species (human and mouse) and cell types (fibroblast or epithelial) (Fig. 2). Always concomitant was a notable increase in ferritin, which may provide a robust biomarker for cellular senescence and for associated iron accumulation (Figs. 3**A,B,**4**C,E,**6**C,D**). In mammalian cells,

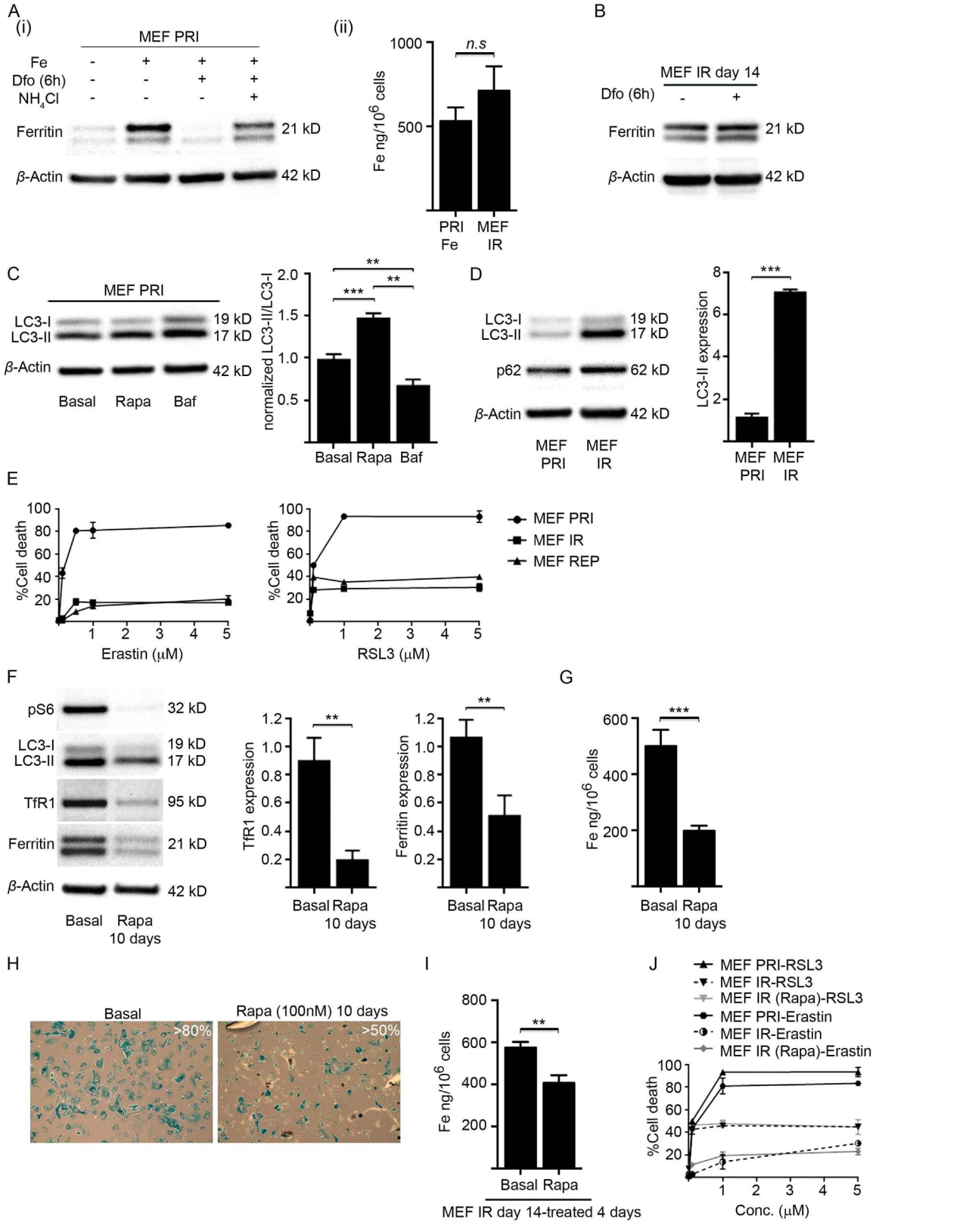


*(caption on next page)*

**Fig. 5.** Iron accumulation in senescent MEFs is associated with impaired ferritinophagy. **(A)** Ferritin degradation in primary MEFs (MEF PRI) was inhibited by lysosomal acidification. **(i)** Primary MEFs (MEF PRI) were treated with 40 μM iron (FAC) for 24 h to increase ferritin expression. Ferritin degradation was stimulated with the iron chelator deferoxamine (Dfo) (50 μM) and occurred substantially with 6 h of treatment, as determined by western blot analyses **(ii)** ICP-MS analyses confirmed that intracellular iron levels increased in primary MEFs following treatment with 40 μM iron (FAC) for 24 h (PRI Fe), subsequently becoming comparable to iron levels observed in senescent MEFs (MEF IR) (14 days post-irradiation).**(B)** Ferritin degradation in senescent MEFs (MEF IR) is impaired. Western blot analysis showing no change to ferritin in senescent MEFs (MEF IR) (14 days post-irradiation) treated with Dfo (50 μM) for 6 h. *β*-actin was detected as a loading control.**(C)** Autophagy in primary MEFs with functional lysosomes can be monitored by the LC3-II: LC3-I ratio. The ratio of LC3-II: LC3-I was determined by western blot analyses and densitometry and increased in primary MEFs (MEF PRI) treated with the autophagy activator rapamycin (100 nM) for 16 h. The ratio of LC3-II: LC3-I was decreased in primary MEFs (MEF PRI) treated with the autophagy inhibitor bafilomycin A1 (100 nM) for 16 h. *β*-actin was detected as a loading control. **(D)** Senescent MEFs (10 days post-irradiation) displayed a large build-up of LC3-II and elevated levels of p62, indicating impaired lysosomal function, as determined by western blot analyses and densitometry. The levels of LC3-II protein and p62 in primary MEFs (MEF PRI) is shown for comparison. *β*-actin was detected as a loading control. **(E)** Senescent MEFs are highly resistant to ferroptosis. The viability of primary and senescent MEFs treated for 24 h with varying concentrations of erastin (0.1–5 μM) and RSL3 (0.1–5 μM) was determined by propidium iodide and flow cytometry. **(F)** Preservation of autophagy averted the accumulation of iron-regulatory proteins in irradiated MEFs. Primary MEFs were treated with rapamycin (100 nM) while irradiated (10 Gy) to become senescent and then subsequently for 10 days in culture. Western blot analyses demonstrated that sustained rapamycin treatment significantly reduced expression of phosphorylated ribosomal protein S6 (pS6). LC3-II levels were likewise significantly reduced indicating preservation of lysosomal function and permissible LC3-II degradation. Rapamycin treatment averted the iron accumulation phenotype of senescent MEFs, preventing the accumulation of TfR1 and ferritin (densitometry shown). *β*-actin was detected as a loading control. **(G)** Preservation of autophagy averted the iron accumulation in irradiated MEFs. Primary MEFs were treated with rapamycin (100 nM) while irradiated (10 Gy) to become senescent and then subsequently for 10 days in culture. Primary MEFs irradiated and cultured in basal medium served as a control. ICP-MS analyses demonstrated that sustained rapamycin treatment averted intracellular iron accumulation in irradiated MEFs. **(H)** Percentage of senescent MEFs following sustained rapamycin treatment. Primary MEFs were treated with rapamycin (100 nM) while irradiated (10 Gy) to become senescent and then subsequently for 10 days in culture. Primary MEFs irradiated and cultured in basal medium served as a control. Approximately 50% of treated MEFs became senescent, staining positive for SA-*β*gal activity as established by blue staining. Images were taken at 100× magnification. **(I)** Autophagy activation reduced stored iron in established senescent MEFs. ICP-MS analyses demonstrated that senescent MEFs (MEF IR) (10 days post-irradiation) treated for 4 days with rapamycin (100 nM) showed a significant reduction in intracellular iron when compared to untreated senescent MEFs (MEF IR). **(J)** Preservation of autophagy was insufficient to sensitize irradiated MEFs to ferroptosis. The viability of primary, senescent, and rapamycin treated irradiated MEFs (MEF IR + Rapa) (as described previously in Fig. 5**G**), treated for 24 h with varying concentrations of erastin and RSL3 (0.1–5 μM) was determined by propidium iodide and flow cytometry. Statistical analysis was performed by student-*t*-test: significant (*$p < 0.05$, **$p < 0.01$, ***$p < 0.001$). Data represented as mean ± SD ($n = 3$).

ferritins assemble to form large (480 kDa) complexes with cavities capable of accommodating up to 4500 atoms of iron and function to modulate iron bioavailability and detoxification within cells [47]. Increased cellular iron uptake positively regulates ferritin expression, both at the transcriptional and translational levels, to afford protection from labile iron-mediated oxidative stress [38]. Most cells subsequently down-regulate iron uptake mechanisms, particularly TfR1 and up-regulate iron efflux via ferroportin in order to regain homeostatic levels (Fig. 4**E(i)**) [47]. However, senescent cells have altered iron homeostatic mechanisms driving both iron acquisition and sustained storage. Senescent cells paradoxically had increased TfR1 and ferritin, coupled with reduced ferroportin at the plasma membrane (Fig. 3**A,**Figs. S2 and S3C). Ferroportin is therefore unlikely to participate in effective iron efflux and consequently iron accumulation prevails through enhanced uptake and sequestration. Senescent cells indeed have an unusual appetite for iron acquisition and can amass remarkable amounts of intracellular iron in comparison to proliferative cells (up to 30-fold increase) (Fig. 4**E(ii),F**).

We established that iron accumulation in senescent cells was associated with autophagic/lysosomal dysfunction (Fig. 5). Autophagy involves the delivery of cytoplasmic substrates (cellular proteins and damaged organelles) to lysosomes for degradation and impairment of this process is associated with premature ageing and age-associated decline in tissue function [58,71]. Autophagy impairment incurred through lysosomal dysfunction has recently been described in cellular senescence and shown to regulate SASP [57,72–75]. Consistent with our findings (Fig. 5**,**Fig. S3), lysosomal dysfunction has been documented in replicative [74] and oxidative stress-induced senescence [57] and in both cases was associated with the buildup of autophagosomes and related markers (e.g. LC3-II, p62). Additionally, lysosomal dysfunction can precede senescence development and drive the associated phenotypic changes [57,73]. Depletion of lysosomal-associated membrane protein 2 (LAMP2), which is critical for fusion between autophagosomes and lysosomes, can induce cellular senescence [57,73], as can pharmacological inhibition of lysosomal activity (hydroxychloroquine & leupeptin treatment) [57]. Furthermore, proteins known to turnover through autophagic degradation accumulate in senescent cells, including the GATA4 transcription factor, an important regulator of SASP [76]. GATA4 in turn activates the NF-*k*B transcription factor to initiate SASP and facilitate senescence progression. Coincidently, impaired autophagy in senescent cells has previously been shown to reduce ferritin turnover, but in this study intracellular iron levels or the levels of major iron homeostasis proteins were not evaluated [77]. Ferritin is selectively targeted for autophagic/lysosomal degradation by the cargo receptor NCOA4 [53], a process required for liberating iron making it bioavailable to the cell [51,53,65]. This process has recently been termed ferritinophagy [53,65]. Promoting ferritin degradation by using the autophagy activator rapamycin averted the iron accumulation phenotype of senescent cells, preventing the increase of TfR1, ferritin and intracellular iron (Fig. 5**F,G**). Additionally, rapamycin treatment may lead to autophagic degradation of TfR1 or modulate levels by enhancing degradation of *TfR1* mRNA [78]. Rapamycin selectively activates autophagy through inhibiting the mTOR pathway [60] and can extend the lifespan of mice [79].

Ferroptosis, a unique cell death pathway distinct from apoptosis [62,66,80], is reliant on the availability of iron [62,66,81] liberated through ferritinophagy [63]. Cells are also desensitized to ferroptosis through genetic silencing of iron uptake (*TfR1*), metabolism (*IRP2* and *ISCU*) and storage (*ferritin*) genes [62,66,82], or through depletion of transferrin in the extracellular environment [83]. Cell death elicited by ferroptosis-inducing compounds (FINs) (e.g. erastin and RSL3) can also be mitigated through various iron chelators (Dfo, 2,2-bipyridile or compound 311) [62,66,81]. Distinctly, ferroptosis can be initiated through repression of the p53 target, SLC7A11, which encodes a component of the cysteine/glutamate antiporter (system Xc-), resulting in iron-dependent accumulation of ROS and glutathione (antioxidant) depletion [62,82]. Erastin induces ferroptosis through silencing SLC7A11 [84] and was recently demonstrated to enhance iron bioavailability through autophagic/lysosomal degradation of ferritin and its cargo receptor NCOA4 [63]. We established that senescent cells were highly resistant to erastin-induced ferroptosis (Fig. 5**E**) and remained refractory despite rapamycin treatment preserving ferritinophagy (Fig. 5**J**). Likewise, senescent cells were also markedly resistant to RSL3 (Fig. 5**E,J**), which in contrast to erastin induces ferroptosis through direct inhibition of glutathione peroxidase 4 (GPX4) without dependance upon system Xc- inhibition or glutathione depletion [82]. What mechanism(s) underpin senescent cell resistance to ferroptosis is under further investigation.

Based on our results we propose the following model to explain iron accumulation in senescent cells. Impaired ferritinophagy traps iron in ferritin creating a perceived cellular deficiency, which in turn causes concomitant changes in the levels of iron regulatory proteins. Elevated IRP2 levels (Fig. 3**C**) are indicative of cellular iron deficiency and stabilizes TfR1 mRNA (via binding to 3′ IRE) increasing its expression to

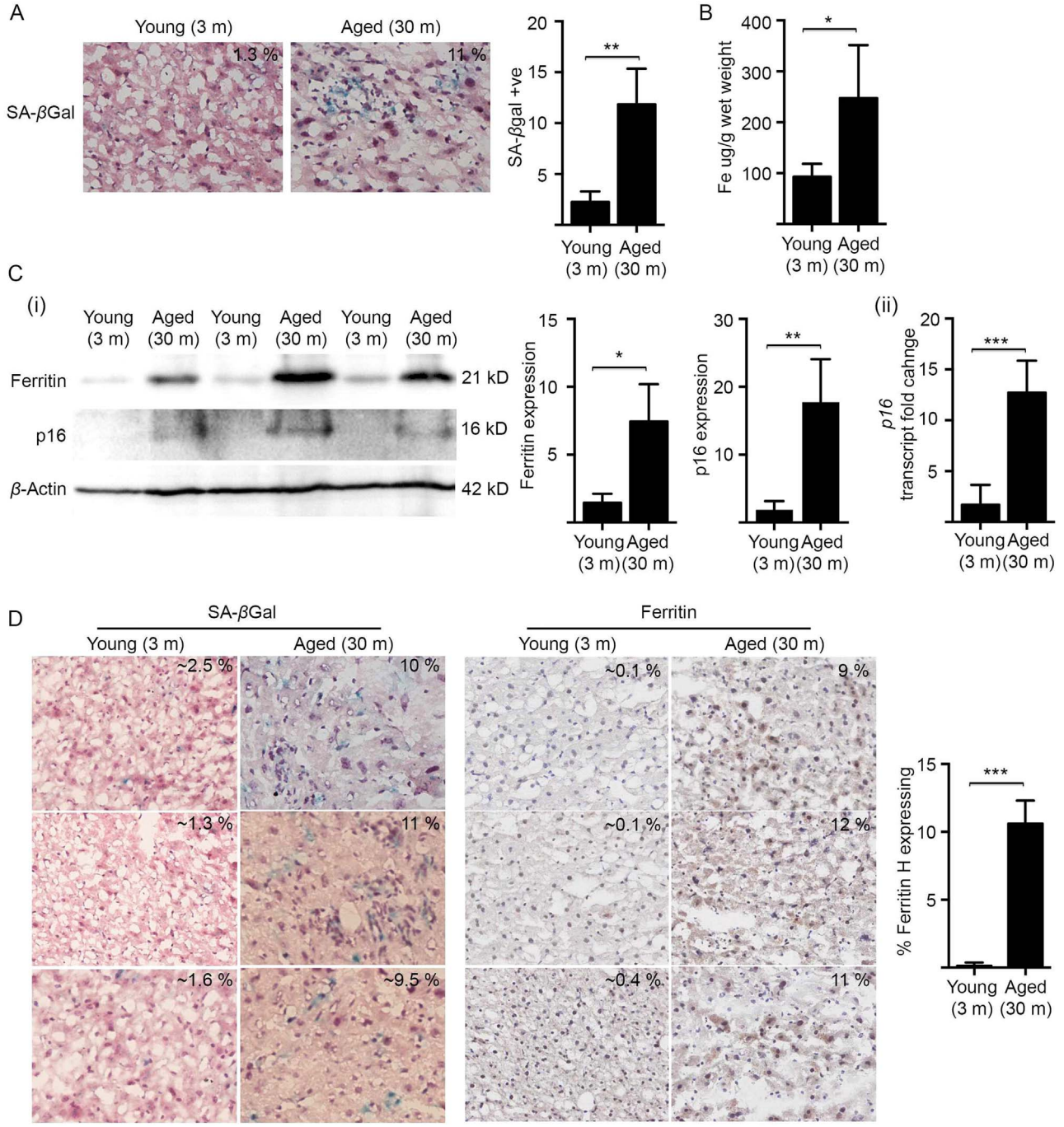


**Fig. 6.** The enrichment of senescent cells in ageing mouse liver is accompanied by iron accumulation and elevated ferritin. **(A)** Senescent cells are markedly enriched in the livers of aged mice. Percentage of senescent cells in serial histological liver sections from both young (3 month; $n = 4$) and aged mice (30 month; $n = 4$) as determined by SA-$\beta$gal activity (blue staining). **(B)** ICP-MS analyses demonstrated a significant increase in iron (~ 2.5-fold) in liver tissues harvested from aged mice (30 month; $n = 4$) when compared to liver tissues harvested from young mice (3 month; $n = 4$). **(C)** The iron-storage protein ferritin and the senescence marker p16 were significantly elevated in livers of aged mice. **(i)** Western blot analyses and densitometry demonstrated that ferritin and p16 expression are increased in liver tissues harvested from aged mice (30 month; $n = 3$) when compared to liver tissues harvested from young mice (3 month; $n = 3$). $\beta$-actin was detected as a loading control. **(ii)** Quantitative real-time PCR analysis confirmed increased *p16* transcript levels in liver tissues harvested from aged mice (30 months, $n = 3$), when compared to liver tissues from young mice (3 months, $n = 3$). **(D)** The percentage of ferritin-enriched cells within aged livers matched the percentage of SA-$\beta$gal positive senescent cells. Serial histological liver sections from both young ($n = 3$) and aged mice ($n = 3$) were stained for either SA-$\beta$gal activity or for ferritin. Images are representative of the mean percentage of either SA-$\beta$gal activity or ferritin staining from each mouse liver, as determined by observing 4 independent fields of view at a magnification of 400X using OlyVIA viewer software (ver2.4). Statistical analysis was performed by student-*t*-test: significant ($*p < 0.05$, $**p < 0.01$, $***p < 0.001$). Data represented as mean ± SD ($n = 3$).

up-regulate cellular iron uptake [48]. However, senescent cells having perturbed ferritin degradation sequester iron (trapped in ferritin), creating a perpetual state of deficiency and a cycle promoting continual iron acquisition. This scenario accounts for the profound iron accumulation observed in senescent cells (up to 20-fold) and for their capacity to extract further iron from enriched media (Fig. 4**E(ii)**). While IRP2 can mediate the degradation of ferritin and ferroportin mRNA [48], this must be insufficient to prevent their biosynthesis in the context of senescent cells. Furthermore, ferritin levels remained responsive in senescent cells, further increasing in iron supplemented

media and affording greater tolerance to iron-induced toxicity (Fig. 4**E (ii), F**). Ferritin and ferroportin can be regulated through mRNA stability or post-translationally through protein turnover [85,86]. Interestingly, ferritin can be upregulated in response to inflammatory cytokines of the SASP (such as IL1 & IL6) that drive translation through an "acute phase box" in the 5′ region of ferritin transcripts [87,88]. Nonetheless, lysosomal dysfunction in senescent cells can account for ferritin and ferroportin accumulation, as both proteins are degraded through the autophagic pathway [51,89]. Consistently, ferroportin predominantly localized at a large intracellular compartment in senescent cells, possibly representing built-up autophagosomes (Fig. S2A). We provided further evidence that senescent cells have a functional iron deficiency, in addition to the observation that they were highly resistant to ferroptosis (Fig. 5**E**). Additionally, ISCU levels are suppressed by iron deprivation, to decrease iron utilization by curtailing iron-sulfur cluster biogenesis [90]. In this situation, IRP1 usually loses its iron-sulfur cluster and aconitase activity and binds IREs with high affinity [48,50]. However, while senescent cells had barely detectable ISCU, consistent with deficient cellular iron, this was coupled with markedly reduced IRP1 and therefore this pathway is unlikely influencing iron regulatory proteins (Fig. 3**C**).

Future studies are required to determine both physiological and pathological roles for iron accumulating in senescent cells. We speculate on one possible physiological function; a probable role in delivering anaemia of inflammation (AI) (a hypoferremic environment) at the site of injury/inflammation to help impede infection [87,91]. The subsequent clearance of iron-laden senescent cells by macrophages [45,92] would then maintain the protective AI and facilitate iron recycling through the reticuloendothelial system [91,93]. Nevertheless, the ramifications of accumulating iron in ageing tissues where senescent cells are enriched would be profound. Conceivably, senescent cells account for the increased iron observed in aged tissues [11,12] and similarly in organs affected by age-related pathologies [13–15]. Furthermore, our findings provide a plausible aetiological link between both senescent cell enrichment and iron dyshomeostasis occurring at the sites of age-related pathologies.

## 4. Materials and methods

### 4.1. Chemicals and reagents

Rapamycin was purchased from Thermo Fischer Scientific (Cat#FSBBP2963-1). Torin 1 was purchased from Cell Signalling Technologies (Cat#14379S). RSL3 was purchased from Jomar Bioscience (Cat# S8155). Erastin (Cat#E7881), ferric ammonium citrate (FAC) (Cat#F5879), deferoxamine mesylate salt (Dfo) (Cat#D9533), deferiprone (Dfp) (Cat#379409), bafilomycin A1 (Baf) (Cat# B1793) and MG-132 (ready made solution) (Cat# M7449) were purchased from Sigma Aldrich. All other reagents were purchased from Sigma Aldrich unless otherwise stated.

### 4.2. Isolation and culturing of primary mouse and human cells

Primary mouse embryonic fibroblasts (MEFs) were collected from sacrificed pregnant wild-type or Li-Fraumeni syndrome C57BL/6 mice at day 13 post-*coitum*, using a protocol modified from that described previously [43]. The Li-Fraumeni syndrome C57BL/6 mice, which carry a germline mutation in *TP53* (G515A nucleotide mutation), were a kind gift from Prof. Guillermina Lozano (University of Texas) [94]. This study was approved by the Deakin University Animal Ethics Committee (AEC) (Id#G01-2014). In brief, intact uteri were removed, washed with cold phosphate-buffered saline (PBS) (without $Ca^{2+}$/$Mg^{2+}$) (Life Technologies, Cat#10010049), and each embryo individually prepared by removing appendages including the head and red organs. A surgical scalpel blade (Size 11, Livingstone) was used to finely mince the remaining tissue, which was then applied through an 18-gauge needle using a 5 mL syringe. Suspended cells derived from each embryo were seeded into separate 10 cm (55 $cm^2$) dishes (Cellstar®, Cat#664160) and cultured in Dulbecco's modified Eagle's medium (DMEM) (Life Technologies, Cat#11965118) supplemented with 10% FBS, penicillin (20 U/mL), streptomycin (20 μg/mL), L-glutamine (2 mM), sodium pyruvate (1 mM), HEPES (1 mM) and non-essential amino acids (1%). When adherent MEFs reached ~ 90% confluency they were expanded into one 14.5 cm (152 $cm^2$) dish (Catalogue no. 639160, Cellstar®), at which stage they were referred to as being passage 2 (P2). Cells were further expanded into three 14.5 cm dishes and subsequently cryopreserved at passage 3 (P3) in liquid $N_2$.

Primary human diploid fibroblasts (HDFs) (S103) isolated from skin by the scratch biopsy method, were obtained from the Murdoch Children's Research Institute, Melbourne, and were collected from healthy control individuals as previously described [95]. HDFs were provided at passage 14 and were cultured in Basal Eagle's medium (BME) supplemented with 10% FBS, penicillin (20 U/mL), streptomycin (20 μg/mL), L-glutamine (4 mM) and HEPES (1 mM). Human primary prostate epithelial cells (PrECs) were purchased from Lonza (Cat#CC-2555) and cultured in the recommended PrEBM growth medium (Cat#CC-3166) and subcultured using reagents provided by the supplier (Cat#CC-5034). All primary cells were incubated at 37 °C in 5% $CO_2$.

### 4.3. Senescence induction by ionizing radiation

Primary mouse and human cell lines (MEFs, HDFs and PRECs) were cultured to ~ 90% confluence in 25 or 75 $cm^2$ flasks (Cellstar®, Cat#690175 or 658175, respectively) and subjected to 10 Gy (Gy) gamma irradiation using a calibrated Cesium-137 source (Gamma Cell 40, Atomic energy of Canada Limited). Primary cells were in their respective standard medium as described above during irradiation. Control non-irradiated cell lines were cultured to equivalent confluence and otherwise handled in the same manner as irradiated cells. Cellular senescence was assessed at various time points (in days) post irradiation by senescence-associated β-galactosidase (SA-βgal) activity staining, as detailed in the Results.

### 4.4. Retrovirus production and transduction of primary MEFs

HEK293T cells were cultured in DMEM medium supplemented with 10% FBS, penicillin (20 U/mL) and streptomycin (20 μg/mL), and were used as a packaging cell line for retrovirus production. The cells were seeded at 5 × $10^6$ cells in a 10 cm (55 $cm^2$) dish and the following day transfected (in 5 mL of medium) with a 500 μL mixture containing 15 μg (total) of plasmid DNA, 45 μL of FuGENE® HD Transfection Reagent (Promega, Cat#E2311) and Opti-MEM medium (Life Technologies, Cat#31985-070). To produce retroviruses containing SV40 Large T antigen (SV40 LgT), equimolar amounts of pBabe-neo large TcDNA plasmid (Addgene, Cat#1780) along with the packaging plasmid pCl-Eco (Addgene, Cat#12371) were used. Retroviruses containing the oncogene *H-Ras$^{V12}$* were produced with pWZL-hygro H-*Ras* V12 plasmid (Addgene, Cat#18749), while control retroviruses were produced with empty pWZL-hygro plasmid (Addgene, Cat#18750). Transfected HEK293T cells were cultured for 24 h before the medium was replaced (5 mL) and subsequently collected every 12 h over a 48 h timeframe. Viral supernatants were pooled, filtered (0.45 μm filter, Millipore) and frozen at − 80 °C until required. Retroviral transduction of MEFs was achieved by culturing 1.2 × $10^6$ cells in a 10 cm (55 $cm^2$) dish overnight, then substituting the medium for 3 h with neat viral supernatant (5 mL) together with polybrene (8 μg/mL). Subsequently, the cells were cultured in fresh medium (10 mL) for 24 h before selection agent (G418; 500 μg/mL or hygromycin 100 μg/mL) was administered.

### 4.5. Senescence-associated β-galactosidase assay in cells and tissues

SA-βgal staining of cultured cells was performed using a protocol modified from that previously described [96]. Adherent cells were washed twice with PBS (30 s each) and then fixed with a PBS solution containing 2% formaldehyde and 0.2% glutaraldehyde for 15 min at room temperature. After a further two PBS washes (30 s each) the cells were incubated in staining solution (150 mM NaCl, 2 mM $MgCl_2$, 5 mM potassium ferricyanide, 5 mM potassium ferrocyanide, 2.45 mM (1 mg/mL) 5-bromo-4-chloro-3-indolyl-β-D-thiogalactopyranoside (X-Gal) in phosphate-citrate buffer, pH 6.0) at 37 °C without $CO_2$ for < 12 h (overnight). The percentage of cells stained for SA-βgal activity was determined using an inverted microscope (Olympus IX51), by counting cells in four random fields of view at a magnification of 200/400X. Images were taken with Canon 1100D digital camera.

SA-βgal staining of tissue sections was performed using a protocol modified from that described previously [97]. Harvested liver from young (3 months) and aged (30 months) mice (wild-type C57BL/6) were frozen immediately on dry ice and stored at − 80 °C until required. Tissue specimens were first attached to cryostat section disks with a drop of optimal cutting temperature compound (OCT) prior to sectioning at − 24 °C. The cryostat was used to cut 5 μm sections, which were then immediately mounted on positively charged slides and fixed in 0.5% glutaraldehyde (in PBS) at room temperature for 15 min. Sections were then rinsed thrice with PBS (1 min each) and incubated in a humidity chamber at 37 °C (without $CO_2$) with fresh SA-βgal staining solution for 8–12 h. The tissue sections were then dehydrated in 90% ethanol (1 min), stained with 1% hematoxylin (1 min) (Thermo Fisher), washed in tap water (30 s) and then rinsed in acidified alcohol (2% 1 N HCl in 90% ethanol) for 3 s. Sections were then washed in tap water (30 s) then in deionized water (30 s) to remove excess stain and rehydrate the samples. Following rehydration the sections were stained in eosin (2%) for 4 min and then rinsed consecutively in 90% ethanol (30 s, twice) and then in 100% ethanol (2 min). Dry sections were then mounted in DPX and a coverslip was applied and the DPX was allowed to dry for 4 h. Using a standard light microscope at a magnification of 400X, SA-βgal stained cells were counted in four random fields for each section together with the total number of cells as determined by haematoxylin stained nuclei. The percentage of senescent cells was determined for tissues harvested from 4 mice per group (young vs. aged) and were averaged to establish the percent of senescent cells in a given tissue. Images were taken with an inverted light microscope (Nikon Eclipse E200) and photographed using an imaging system (Nikon digital site, DS-Fi1).

### 4.6. Western blotting analyses

Cell cultures were washed once and harvested with trypsin-EDTA solution (0.025% trypsin with 0.02% EDTA) and pelleted by centrifugation at 5000 × *g*. RIPA buffer (50 mM Tris, 150 mM NaCl, 0.1% SDS, 0.5% sodium deoxycholate, 1% Triton X-100 and a protease inhibitor cocktail tablet (Roche)) was then used to lyse the cell pellet ($5 \times 10^5$ cells per 150 μL of RIPA buffer), which was incubated on ice for 10 min before being centrifuged at 10,000 × *g* for 10 min at 4 °C to remove insoluble cell debris. Protein concentration was determined by the BCA protein assay kit (Thermo Scientific) as per the manufacturer's instructions. Total cell lysates were made up in SDS protein sample buffer (final concentrations: 50 mM Tris/HCl, 2% (w/v) SDS, 0.1% Bromophenol Blue, 10% glycerol and 10% β-mercaptoethanol). NP-40 insoluble fractions were prepared as described previously [98]. To obtain enriched plasma membrane fractions, cell pellets were suspended in 500 μL of homogenization buffer (250 mM sucrose, 10 mM HEPES pH 7.5 with protease inhibitor cocktail tablet), followed by sonication (Fisher Scientific Model 550 Sonic Dismembrator) using a microtip probe (amplitude setting 2, two cycles of 15 s). Samples were then centrifuged at 1500 × *g* for 15 min at 4 °C to remove insoluble cell debris. Supernatant was transferred to 4.7 mL polyallomer centrifuge tubes with plugs (OptiSeal™ tubes, Beckman Coulter) and filled with excess homogenization buffer and centrifuged at 48,000 × *g* for 1 h at 4 °C. The plasma membrane pellet obtained was then resuspended in 100 μL solubilisation buffer (62.5 mM Tris-HCl pH 6.8, 5% SDS) by heating to 50 °C. Protein concentration was determined as described above. Plasma membrane enriched lysates were made up in SDS protein sample buffer.

Freshly harvested liver tissues were frozen on dry ice and stored at − 80 °C until required. Each tissue was ground using a pre-chilled (in liquid $N_2$) mortar and pestle as previously described [99]. Resultant dry powder was then transferred to pre-chilled 1.5 mL microcentrifuge tubes. Powdered tissue (50 mg) was then lysed in RIPA buffer (500 μL) and incubated on ice for 10 min. Tissue lysate was homogenized by passing consecutively through 25 and 21 gauge needles and then by sonication (Fisher Scientific Model 550 Sonic Dismembrator) using a microtip probe (amplitude setting 2, two cycles of 15 s). The lysate was then centrifuged at 12,000 × *g* for 10 min to remove insoluble debris and either frozen at − 80 °C or used immediately for protein estimation (BCA method) and western blotting.

Proteins samples (30–50 μg) were fractionated using the Novex Bolt® Mini-Gel system (Bio-Rad Technologies) on Bolt® 4–12% Bis-Tris Plus precast gels and transferred to nitrocellulose membrane using Bolt® transfer system and buffer containing Tris-HCl (25 mM), glycine (192 mM) and 15% methanol (10% for IRP2). Membranes were blocked for 1 h at room temperature using 5% (w/v) skimmed milk in wash (TBS-T) buffer containing Tris-HCl [10 mM (pH 8.0), NaCl (150 mM) and 0.1% Tween-20]. The following antibody dilutions were used: Anti-p16 (Cat#sc-1207, 1:1000), was purchased from Santa Cruz Biotechnology, USA. Anti-β-actin (Cat#A5441, 1:10000), anti-LC3B (Cat#L7543, 1:1000) and HRP conjugated anti-goat IgG (Cat#A5420, 1:5000) were purchased from Sigma Aldrich. Anti-SV40 Large T antigen (Cat#MABF121, 1:4000) was purchased from Merck Millipore. Anti-ferritin (Cat#EPR3004Y, 1:1000), anti-IRP1 (Cat#EPR7225, 1:1000) and anti-p53 (Cat#PAb 240, 1:1000) were purchased from Abcam. Anti-TfR1 (H68.4, 1:1000) was purchased from Invitrogen. Anti-IRP2 (Cat#NB100-1798, 1:1000) was purchased from Novus Biologicals. Anti-DMT1 (Cat#NRAMP21-P, 1:1000) was purchased from Alpha Diagnostics International. Anti-ferroportin (MAP 23, 1:1000) was kindly provided by Dr. Bruce Wong (Department of Pathology, University of Melbourne). Anti-ISCU (Cat#14812-1-AP, 1:1000) and anti-p16 (Cat#10883-1-AP, 1:500) was purchased from Proteintech. Anti-phospho S6 ribosomal protein (pS6) (Cat#2211S) and anti-p62 (Cat#5114T) were purchased from Cell Signalling Technologies. HRP conjugated goat-anti-mouse (Cat#P0447) and goat-anti-rabbit (Cat#P0448) antibodies were purchased from Dako. The membranes was subsequently developed using ECL reagent (Millipore, Cat#WBKLS0500) and bands visualized on Gel Dock™ XR+ system (Bio-Rad). At least three independent experiments were used for all comparisons.

### 4.7. Determination of total intracellular iron

Total metal concentration was measured using inductively coupled plasma mass spectrometry (ICP-MS, Agilent 7700, Varian). Tissue culture cells were prepared for ICP-MS analyses as previously described [100]. In brief, the cells were washed with 5 mL of trypsin-EDTA solution before being harvested with 5 mL of trypsin-EDTA solution for a 10 cm dish or 75 $cm^2$ flask. Suspended cells were counted using a Beckman Coulter Z Series Cell Count and Size Analyser. Four 1 mL aliquots of the cell suspension were centrifuged at 1000 × *g* for 5 min at room temperature to pellet the cells and subsequently stored at − 80 °C until required. Tissue samples were weighed and prepared for ICP-MS analyses as previously described [100]. Quadruplicate determinations of iron concentration was performed for each sample. Unit conversions from raw ppb values were performed as follows: Cell culture (ng/

million cells) = (raw ppb values × dilution factor/cell number); Tissue (μg/g) = (raw ppb value × dilution factor × reduced digest volume / tissue wet weight g).

### 4.8. Immunohistochemistry

Cryosections 5 μm thick were fixed in formalin. Endogenous peroxidase was quenched with 3% hydrogen peroxidase in distilled water. Non-specific binding was blocked using TNB buffer (0.1 M Tris-HCl, pH 7.5, 0.15 M NaCl, 0.5% (w/v) blocking reagent, PerkinElmer FP1020). Sections were incubated in Rabbit polyclonal anti-ferritin antibody (Santa Cruz, Cat#sc-25617) or a Rabbit IgG control (Abcam, Cat#ab27478) at a dilution of 2 μg/mL. To visualise the distribution of ferritin, sections were incubated with ImmPRESSTM HRP anti-rabbit IgG (Vector Laboratories, Cat#MP-7401) and 3, 3'-diaminobenzidine (DAKO, Cat# K3468) according to the manufacturer's instructions. Sections were counterstained in haematoxylin before coverslipping.

### 4.9. Cell viability assay

Adhered cells were harvested using trypsin-EDTA solution (0.025% trypsin and 0.02% EDTA) and then combined with their corresponding conditioned medium in 5 mL flow cytometry tubes. Cells were pelleted by centrifugation at 1000 × *g* for 5 min at 4 °C. To determine cell viability, cell pellets were resuspended in 200 μL of PBS containing 5 μg/mL propidium iodide (PI, excitation 538 nm/emission 617 nm) and immediately analysed with a FACS Canto II flow cytometer (BD Biosciences). 10,000 events were measured and the percentage of dead cells (cells positive for PI) was determined.

### 4.10. Statistical and image analyses

Statistical analyses were performed using two-tailed unpaired *t*-tests, calculated on GraphPad PRISM (version 6.0b) software. All data are represented as mean ± SD; probabilities of $P < 0.05$ were considered significant.

## Author contributions

Masaldan S designed and conducted most of the experiments. Clatworthy SAS, Meggyesy P and Rigopoulos A-T helped with data collection. Gamell C, Haupt S and Haupt Y helped conduct IR and p53-related experiments. Denoyer D helped conduct cell viability assays and data collection. Adlard P and Bush AI provided aged mice and tissues and helped design experiments. Cater MA designed, funded and supervised the project. Masaldan S and Cater MA wrote the manuscript.

## Acknowledgments

The authors would like to thank Prof Sarah Ellis (University of Melbourne, Australia) for providing support with histological analyses. We also thank Ms Irene Volitakis (University of Melbourne, Australia) for ICP-MS analyses, Luke Amor from the Deakin University Animal Facility for technical support, and Dr. Scott Ayton and Dr. Abdel Belaidi (University of Melbourne, Australia) for helpful feedback on experiments. This study was funded by the National Health and Medical Research Council of Australia (NHMRC) (1027125) (M.A. Cater) and by Deakin University (M.A. Cater).

## Appendix A. Supplementary material

Supplementary data associated with this article can be found in the online version at http://dx.doi.org/10.1016/j.redox.2017.08.015.

## References

[1] J. Campisi, L. Robert, Cell senescence: role in aging and age-related diseases, Interdiscip. Top. Gerontol. 39 (2014) 45–61.
[2] J.M. van Deursen, The role of senescent cells in ageing, Nature 509 (7501) (2014) 439–446.
[3] D.J. Baker, B.G. Childs, M. Durik, M.E. Wijers, C.J. Sieben, J. Zhong, et al., Naturally occurringp16(Ink4a)-positive cells shorten healthy lifespan, Nature 530 (7589) (2016) 184–189.
[4] D.J. Baker, T. Wijshake, T. Tchkonia, N.K. LeBrasseur, B.G. Childs, B. van de Sluis, et al., Clearance of p16Ink4a-positive senescent cells delays ageing-associated disorders, Nature 479 (7372) (2011) 232–236.
[5] I.B. Roninson, Tumor cell senescence in cancer treatment, Cancer Res. 63 (11) (2003) 2705–2715.
[6] M.P. Baar, R.M.C. Brandt, D.A. Putavet, J.D.D. Klein, K.W.J. Derks, B.R.M. Bourgeois, et al., Targeted apoptosis of senescent cells restores tissue homeostasis in response to chemotoxicity and aging, Cell 169 (1) (2017) 132–147 (e16).
[7] H.K. Sanoff, A.M. Deal, J. Krishnamurthy, C. Torrice, P. Dillon, J. Sorrentino, et al., Effect of cytotoxic chemotherapy on markers of molecular age in patients with breast cancer, J. Natl. Cancer Inst. 106 (4) (2014) dju057.
[8] J.A. Ewald, J.A. Desotelle, G. Wilding, D.F. Jarrard, Therapy-induced senescence in cancer, J. Natl. Cancer Inst. 102 (20) (2010) 1536–1546.
[9] M. Demaria, M.N. O'Leary, J. Chang, L. Shao, S. Liu, F. Alimirah, et al., Cellular senescence promotes adverse effects of chemotherapy and cancer relapse, Cancer Discov. 7 (2) (2017) 165–176.
[10] Y. Sun, J. Campisi, C. Higano, T.M. Beer, P. Porter, I. Coleman, et al., Treatment-induced damage to the tumor microenvironment promotes prostate cancer therapy resistance through WNT16B, Nat. Med. 18 (9) (2012) 1359–1368.
[11] S.J. Fairweather-Tait, A.A. Wawer, R. Gillings, A. Jennings, P.K. Myint, Iron status in the elderly, Mech. Ageing Dev. 136–137 (2014) 22–28.
[12] J. Xu, Z. Jia, M.D. Knutson, C. Leeuwenburgh, Impaired iron status in aging research, Int. J. Mol. Sci. 13 (2) (2012) 2368–2386.
[13] E. Puxeddu, A. Comandini, F. Cavalli, G. Pezzuto, C. D'Ambrosio, L. Senis, et al., Iron laden macrophages in idiopathic pulmonary fibrosis: the telltale of occult alveolar hemorrhage? Pulm. Pharmacol. Ther. 28 (1) (2014) 35–40.
[14] D.J. Ogilvie-Harris, V.L. Fornaiser, Synovial iron deposition in osteoarthritis and rheumatoid arthritis, J. Rheumatol. 7 (1) (1980) 30–36.
[15] C. Morris, D. Blake, A. Wainwright, M. Steven, Relationship between iron deposits and tissue damage in the synovium: an ultrastructural study, Ann. Rheum. Dis. 45 (1) (1986) 21–26.
[16] P. Hahn, Y. Song, G.S. Ying, X. He, J. Beard, J.L. Dunaief, Age-dependent and gender-specific changes in mouse tissue iron by strain, Exp. Gerontol. 44 (9) (2009) 594–600.
[17] J.R. Connor, B.S. Snyder, J.L. Beard, R.E. Fine, E.J. Mufson, Regional distribution of iron and iron-regulatory proteins in the brain in aging and Alzheimer's disease, J. Neurosci. Res. 31 (2) (1992) 327–335.
[18] P. Hahn, G.S. Ying, J. Beard, J.L. Dunaief, Iron levels in human retina: sex difference and increase with age, Neuroreport 17 (17) (2006) 1803–1806.
[19] C.I. Cook, B.P. Yu, Iron accumulation in aging: modulation by dietary restriction, Mech. Ageing Dev. 102 (1) (1998) 1–13.
[20] S.J. Chinta, G. Woods, A. Rane, M. Demaria, J. Campisi, J.K. Andersen, Cellular senescence and the aging brain, Exp. Gerontol. 68 (2015) 3–7.
[21] R. Bhat, E.P. Crowe, A. Bitto, M. Moh, C.D. Katsetos, F.U. Garcia, et al., Astrocyte senescence as a component of Alzheimer's disease, PLoS One 7 (9) (2012) e45069.
[22] S.J. Chinta, C.A. Lieu, M. Demaria, R.M. Laberge, J. Campisi, J.K. Andersen, Environmental stress, ageing and glial cell senescence: a novel mechanistic link to Parkinson's disease? J. Intern. Med. 273 (5) (2013) 429–436.
[23] J. Rose, S. Soder, C. Skhirtladze, N. Schmitz, P.M. Gebhard, S. Sesselmann, et al., DNA damage, discoordinated gene expression and cellular senescence in osteoarthritic chondrocytes, Osteoarthr. Cartil. 20 (9) (2012) 1020–1028.
[24] D. Philipot, D. Guerit, D. Platano, P. Chuchana, E. Olivotto, F. Espinoza, et al., P16INK4a and its regulator miR-24 link senescence and chondrocyte terminal differentiation-associated matrix remodeling in osteoarthritis, Arthritis Res. Ther. 16 (1) (2014) R58.
[25] M.J. Schafer, T.A. White, K. Iijima, A.J. Haak, G. Ligresti, E.J. Atkinson, et al., Cellular senescence mediates fibrotic pulmonary disease, Nat. Commun. 8 (2017) 14532.
[26] R.J. Ward, F.A. Zucca, J.H. Duyn, R.R. Crichton, L. Zecca, The role of iron in brain ageing and neurodegenerative disorders, Lancet Neurol. 13 (10) (2014) 1045–1060.
[27] W.Z. Zhu, W.D. Zhong, W. Wang, C.J. Zhan, C.Y. Wang, J.P. Qi, et al., Quantitative MR phase-corrected imaging to investigate increased brain iron deposition of patients with Alzheimer disease, Radiology 253 (2) (2009) 497–504.
[28] G. Bartzokis, T.A. Tishler, I.S. Shin, P.H. Lu, J.L. Cummings, Brain ferritin iron as a risk factor for age at onset in neurodegenerative diseases, Ann. N.Y. Acad. Sci. 1012 (2004) 224–236.
[29] S. Ayton, P. Lei, P.A. Adlard, I. Volitakis, R.A. Cherny, A.I. Bush, et al., Iron accumulation confers neurotoxicity to a vulnerable population of nigral neurons: implications for Parkinson's disease, Mol. Neurodegener. 9 (2014) 27.
[30] D.T. Dexter, F.R. Wells, F. Agid, Y. Agid, A.J. Lees, P. Jenner, et al., Increased nigral iron content in postmortem parkinsonian brain, Lancet 2 (8569) (1987) 1219–1220.
[31] J. Lhermitte, W.M. Kraus, D. McAlpine, Original papers: on the occurrence of abnormal deposits of iron in the brain in parkinsonism with special reference to its localisation, J. Neurol. Psychopathol. 5 (19) (1924) 195–208.
[32] P. Fritz, J. Saal, C. Wicherek, A. König, W. Laschner, H. Rautenstrauch, Quantitative

photometrical assessment of iron deposits in synovial membranes in different joint diseases, Rheumatol. Int. 15 (5) (1996) 211–216.
[33] A. Camacho, M. Simão, H.-K. Ea, M. Cohen-Solal, P. Richette, J. Branco, et al., Iron overload in a murine model of hereditary hemochromatosis is associated with accelerated progression of osteoarthritis under mechanical stress, Osteoarthr. Cartil. 24 (3) (2016) 494–502.
[34] D.B. Chandler, J.C. Barton, D.D. Briggs 3rd, T.W. Butler, J.I. Kennedy, W.E. Grizzle, et al., Effect of iron deficiency on bleomycin-induced lung fibrosis in the hamster, Am. Rev. Respir. Dis. 137 (1) (1988) 85–89.
[35] D.W. Killilea, H. Atamna, C. Liao, B.N. Ames, Iron accumulation during cellular senescence in human fibroblasts in vitro, Antioxid. Redox Signal. 5 (5) (2003) 507–516.
[36] C. Ott, J. Konig, A. Hohn, T. Jung, T. Grune, Macroautophagy is impaired in old murine brain tissue as well as in senescent human fibroblasts, Redox Biol. 10 (2016) 266–273.
[37] K.C. DeRuisseau, Y.M. Park, L.R. DeRuisseau, P.M. Cowley, C.H. Fazen, R.P. Doyle, Aging-related changes in the iron status of skeletal muscle, Exp. Gerontol. 48 (11) (2013) 1294–1302.
[38] A. Freund, R.M. Laberge, M. Demaria, J. Campisi, Lamin B1 loss is a senescence-associated biomarker, Mol. Biol. Cell. 23 (11) (2012) 2066–2075.
[39] J. Cmielova, R. Havelek, T. Soukup, A. Jiroutova, B. Visek, J. Suchanek, et al., Gamma radiation induces senescence in human adult mesenchymal stem cells from bone marrow and periodontal ligaments, Int. J. Radiat. Biol. 88 (5) (2012) 393–404.
[40] B.G. Childs, M. Durik, D.J. Baker, J.M. van Deursen, Cellular senescence in aging and age-related disease: from mechanisms to therapy, Nat. Med. 21 (12) (2015) 1424–1435.
[41] T. Kuilman, C. Michaloglou, W.J. Mooi, D.S. Peeper, The essence of senescence, Genes Dev. 24 (22) (2010) 2463–2479.
[42] R. Milo, What is the total number of protein molecules per cell volume? A call to rethink some published values, Bioessay.: News Rev. Mol. Cell. Dev. Biol. 35 (12) (2013) 1050–1055.
[43] G.J. Todaro, H. Green, Quantitative studies of the growth of mouse embryo cells in culture and their development into established lines, J. Cell Biol. 17 (1963) 299–313.
[44] M. Serrano, A.W. Lin, M.E. McCurrach, D. Beach, S.W. Lowe, Oncogenic ras provokes premature cell senescence associated with accumulation of p53 and p16INK4a, Cell 88 (5) (1997) 593–602.
[45] M. Storer, A. Mas, A. Robert-Moreno, M. Pecoraro, M.C. Ortells, V. Di Giacomo, et al., Senescence is a developmental mechanism that contributes to embryonic growth and patterning, Cell 155 (5) (2013) 1119–1130.
[46] S.J. Dixon, B.R. Stockwell, The role of iron and reactive oxygen species in cell death, Nat. Chem. Biol. 10 (1) (2014) 9–17.
[47] E.L. MacKenzie, K. Iwasaki, Y. Tsuji, Intracellular iron transport and storage: from molecular mechanisms to health implications, Antioxid. Redox Signal. 10 (6) (2008) 997–1030.
[48] T.A. Rouault, The role of iron regulatory proteins in mammalian iron homeostasis and disease, Nat. Chem. Biol. 2 (8) (2006) 406–414.
[49] Y. Funauchi, C. Tanikawa, P.H. Yi Lo, J. Mori, Y. Daigo, A. Takano, et al., Regulation of iron homeostasis by the p53-ISCU pathway, Sci. Rep. 5 (2015) 16497.
[50] T.A. Rouault, Mammalian iron-sulphur proteins: novel insights into biogenesis and function, Nat. Rev. Mol. Cell Biol. 16 (1) (2015) 45–55.
[51] T. Asano, M. Komatsu, Y. Yamaguchi-Iwai, F. Ishikawa, N. Mizushima, K. Iwai, Distinct mechanisms of ferritin delivery to lysosomes in iron-depleted and iron-replete cells, Mol. Cell. Biol. 31 (10) (2011) 2040–2052.
[52] K. Iwai, R.D. Klausner, T.A. Rouault, Requirements for iron-regulated degradation of the RNA binding protein, iron regulatory protein 2, EMBO J. 14 (21) (1995) 5350–5357.
[53] J.D. Mancias, X. Wang, S.P. Gygi, J.W. Harper, A.C. Kimmelman, Quantitative proteomics identifies NCOA4 as the cargo receptor mediating ferritinophagy, Nature 509 (7498) (2014) 105–109.
[54] T.Z. Kidane, E. Sauble, M.C. Linder, Release of iron from ferritin requires lysosomal activity, Am. J. Physiol. Cell Physiol. 291 (3) (2006) C445–C455.
[55] Y. Zhang, M. Mikhael, D. Xu, Y. Li, S. Soe-Lin, B. Ning, et al., Lysosomal proteolysis is the primary degradation pathway for cytosolic ferritin and cytosolic ferritin degradation is necessary for iron exit, Antioxid. Redox Signal. 13 (7) (2010) 999–1009.
[56] I. De Domenico, D.M. Ward, J. Kaplan, Specific iron chelators determine the route of ferritin degradation, Blood 114 (20) (2009) 4546–4551.
[57] H. Tai, Z. Wang, H. Gong, X. Han, J. Zhou, X. Wang, et al., Autophagy impairment with lysosomal and mitochondrial dysfunction is an important characteristic of oxidative stress-induced senescence, Autophagy 13 (1) (2017) 99–113.
[58] I. Tanida, N. Minematsu-Ikeguchi, T. Ueno, E. Kominami, Lysosomal turnover, but not a cellular level, of endogenous LC3 is a marker for autophagy, Autophagy 1 (2) (2005) 84–91.
[59] N. Mizushima, T. Yoshimori, How to interpret LC3 immunoblotting, Autophagy 3 (6) (2007) 542–545.
[60] S. Sarkar, B. Ravikumar, R.A. Floto, D.C. Rubinsztein, Rapamycin and mTOR-independent autophagy inducers ameliorate toxicity of polyglutamine-expanded huntingtin and related proteinopathies, Cell Death Differ. 16 (1) (2009) 46–56.
[61] A. Yamamoto, Y. Tagawa, T. Yoshimori, Y. Moriyama, R. Masaki, Y. Tashiro, Bafilomycin A1 prevents maturation of autophagic vacuoles by inhibiting fusion between autophagosomes and lysosomes in rat hepatoma cell line, H-4-II-E cells, Cell Struct. Funct. 23 (1) (1998) 33–42.
[62] S.J. Dixon, K.M. Lemberg, M.R. Lamprecht, R. Skouta, E.M. Zaitsev, C.E. Gleason, et al., Ferroptosis: an iron-dependent form of nonapoptotic cell death, Cell 149 (5) (2012) 1060–1072.
[63] M. Gao, P. Monian, Q. Pan, W. Zhang, J. Xiang, X. Jiang, Ferroptosis is an autophagic cell death process, Cell Res. 26 (9) (2016) 1021–1032.
[64] A.J. Wolpaw, K. Shimada, R. Skouta, M.E. Welsch, U.D. Akavia, D. Pe'er, et al., Modulatory profiling identifies mechanisms of small molecule-induced cell death, Proc. Natl. Acad. Sci. USA 108 (39) (2011) E771–E780.
[65] W. Hou, Y. Xie, X. Song, X. Sun, M.T. Lotze, H.J. Zeh 3rdet al., Autophagy promotes ferroptosis by degradation of ferritin, Autophagy 12 (8) (2016) 1425–1428.
[66] W.S. Yang, B.R. Stockwell, Synthetic lethal screening identifies compounds activating iron-dependent, nonapoptotic cell death in oncogenic-RAS-harboring cancer cells, Chem. Biol. 15 (3) (2008) 234–245.
[67] S. Xu, Y. Cai, Y. Wei, mTOR signaling from cellular senescence to organismal aging, Aging Dis. 5 (4) (2014) 263–273.
[68] R.M. Laberge, Y. Sun, A.V. Orjalo, C.K. Patil, A. Freund, L. Zhou, et al., MTOR regulates the pro-tumorigenic senescence-associated secretory phenotype by promoting IL1A translation, Nat. Cell Biol. 17 (8) (2015) 1049–1061.
[69] E.F. Blommaart, J.J. Luiken, P.J. Blommaart, G.M. van Woerkom, A.J. Meijer, Phosphorylation of ribosomal protein S6 is inhibitory for autophagy in isolated rat hepatocytes, J. Biol. Chem. 270 (5) (1995) 2320–2326.
[70] Y.C. Kim, K.L. Guan, MTOR: a pharmacologic target for autophagy regulation, J. Clin. Investig. 125 (1) (2015) 25–32.
[71] D.C. Rubinsztein, G. Marino, G. Kroemer, Autophagy and aging, Cell 146 (5) (2011) 682–695.
[72] X. Han, H. Tai, X. Wang, Z. Wang, J. Zhou, X. Wei, et al., AMPK activation protects cells from oxidative stress-induced senescence via autophagic flux restoration and intracellular NAD(+) elevation, Aging Cell 15 (3) (2016) 416–427.
[73] H.T. Kang, K.B. Lee, S.Y. Kim, H.R. Choi, S.C. Park, Autophagy impairment induces premature senescence in primary human fibroblasts, PLoS One 6 (8) (2011) e23367.
[74] J.R. Lin, W.L. Shen, C. Yan, P.J. Gao, Downregulation of dynamin-related protein 1 contributes to impaired autophagic flux and angiogenic function in senescent endothelial cells, Arterioscler. Thromb. Vasc. Biol. 35 (6) (2015) 1413–1422.
[75] Y. Mizunoe, Y. Sudo, N. Okita, H. Hiraoka, K. Mikami, T. Narahara, et al., Involvement of lysosomal dysfunction in autophagosome accumulation and early pathologies in adipose tissue of obese mice, Autophagy 0 (2017).
[76] C. Kang, Q. Xu, T.D. Martin, M.Z. Li, M. Demaria, L. Aron, et al., The DNA damage response induces inflammation and senescence by inhibiting autophagy of GATA4, Science 349 (6255) (2015) aaa5612.
[77] C. Ott, J. Konig, A. Hohn, T. Jung, T. Grune, Reduced autophagy leads to an impaired ferritin turnover in senescent fibroblasts, Free Radic. Biol. Med. 101 (2016) 325–333.
[78] M. Bayeva, A. Khechaduri, S. Puig, H.C. Chang, S. Patial, P.J. Blackshear, et al., mTOR regulates cellular iron homeostasis through tristetraprolin, Cell Metab. 16 (5) (2012) 645–657.
[79] D.E. Harrison, R. Strong, Z.D. Sharp, J.F. Nelson, C.M. Astle, K. Flurkey, et al., Rapamycin fed late in life extends lifespan in genetically heterogeneous mice, Nature 460 (7253) (2009) 392–395.
[80] N. Yagoda, M. von Rechenberg, E. Zaganjor, A.J. Bauer, W.S. Yang, D.J. Fridman, et al., RAS-RAF-MEK-dependent oxidative cell death involving voltage-dependent anion channels, Nature 447 (7146) (2007) 864–868.
[81] J.C. Reed, M. Pellecchia, Ironing out cell death mechanisms, Cell 149 (5) (2012) 963–965.
[82] J.Y. Cao, S.J. Dixon, Mechanisms of ferroptosis, Cell. Mol. Life Sci.: CMLS 73 (11–12) (2016) 2195–2209.
[83] M. Gao, P. Monian, N. Quadri, R. Ramasamy, X. Jiang, Glutaminolysis and transferrin regulate ferroptosis, Mol. Cell 59 (2) (2015) 298–308.
[84] S.J. Dixon, D.N. Patel, M. Welsch, R. Skouta, E.D. Lee, M. Hayano, et al., Pharmacological inhibition of cystine-glutamate exchange induces endoplasmic reticulum stress and ferroptosis, eLife 3 (2014) e02523.
[85] D.M. Ward, J. Kaplan, Ferroportin-mediated iron transport: expression and regulation, Biochim. Biophys. Acta 1823 (9) (2012) 1426–1433.
[86] J.W. Drysdale, H.N. Munro, Regulation of synthesis and turnover of ferritin in rat liver, J. Biol. Chem. 241 (15) (1966) 3630–3637.
[87] M. Wessling-Resnick, Iron homeostasis and the inflammatory response, Annu. Rev. Nutr. 30 (2010) 105–122.
[88] M. Kobune, Y. Kohgo, J. Kato, E. Miyazaki, Y. Niitsu, Interleukin-6 enhances hepatic transferrin uptake and ferritin expression in rats, Hepatology 19 (6) (1994) 1468–1475.
[89] E. Nemeth, M.S. Tuttle, J. Powelson, M.B. Vaughn, A. Donovan, D.M. Ward, et al., Hepcidin regulates cellular iron efflux by binding to ferroportin and inducing its internalization, Science 306 (5704) (2004) 2090–2093.
[90] W.H. Tong, T.A. Rouault, Functions of mitochondrial ISCU and cytosolic ISCU in mammalian iron-sulfur cluster biogenesis and iron homeostasis, Cell Metab. 3 (3) (2006) 199–210.
[91] T. Ganz, E. Nemeth, Iron homeostasis in host defence and inflammation, Nat. Rev. Immunol. 15 (8) (2015) 500–510.
[92] D. Munoz-Espin, M. Canamero, A. Maraver, G. Gomez-Lopez, J. Contreras, S. Murillo-Cuesta, et al., Programmed cell senescence during mammalian embryonic development, Cell 155 (5) (2013) 1104–1118.
[93] T. Ganz, Macrophages and systemic iron homeostasis, J. Innate Immun. 4 (5–6) (2012) 446–453.
[94] G.A. Lang, T. Iwakuma, Y.A. Suh, G. Liu, V.A. Rao, J.M. Parant, et al., Gain of function of a p53 hot spot mutation in a mouse model of Li-Fraumeni syndrome, Cell 119 (6) (2004) 861–872.
[95] A. Michalczyk, G. Varigos, A. Catto-Smith, R.C. Blomeley, M.L. Ackland, Analysis of zinc transporter, hZnT4 ( Slc30A4), gene expression in a mammary gland disorder leading to reduced zinc secretion into milk, Hum. Genet. 113 (3) (2003) 202–210.

[96] G.P. Dimri, X. Lee, G. Basile, M. Acosta, G. Scott, C. Roskelley, et al., A biomarker that identifies senescent human cells in culture and in aging skin in vivo, Proc. Natl. Acad. Sci. USA 92 (20) (1995) 9363–9367.
[97] G.W. Hinkal, C.E. Gatza, N. Parikh, L.A. Donehower, Altered senescence, apoptosis, and DNA damage response in a mutant p53 model of accelerated aging, Mech. Ageing Dev. 130 (4) (2009) 262–271.
[98] M.A. Cater, Y. Haupt, Clioquinol induces cytoplasmic clearance of the X-linked inhibitor of apoptosis protein (XIAP): therapeutic indication for prostate cancer, Biochem. J. 436 (2) (2011) 481–491.
[99] B.X. Ke, R.M. Llanos, M. Wright, Y. Deal, J.F. Mercer, Alteration of copper physiology in mice overexpressing the human Menkes protein ATP7A, Am. J. Physiol. Regul. Integr. Comp. Physiol. 290 (5) (2006) R1460–R1467.
[100] D. Denoyer, H.B. Pearson, S.A. Clatworthy, Z.M. Smith, P.S. Francis, R.M. Llanos, et al., Copper as a target for prostate cancer therapeutics: copper-ionophore pharmacology and altering systemic copper distribution, Oncotarget (2016).